iScience

CellPress

Article

Direct microRNA Sequencing Using Nanopore-Induced Phase-Shift Sequencing

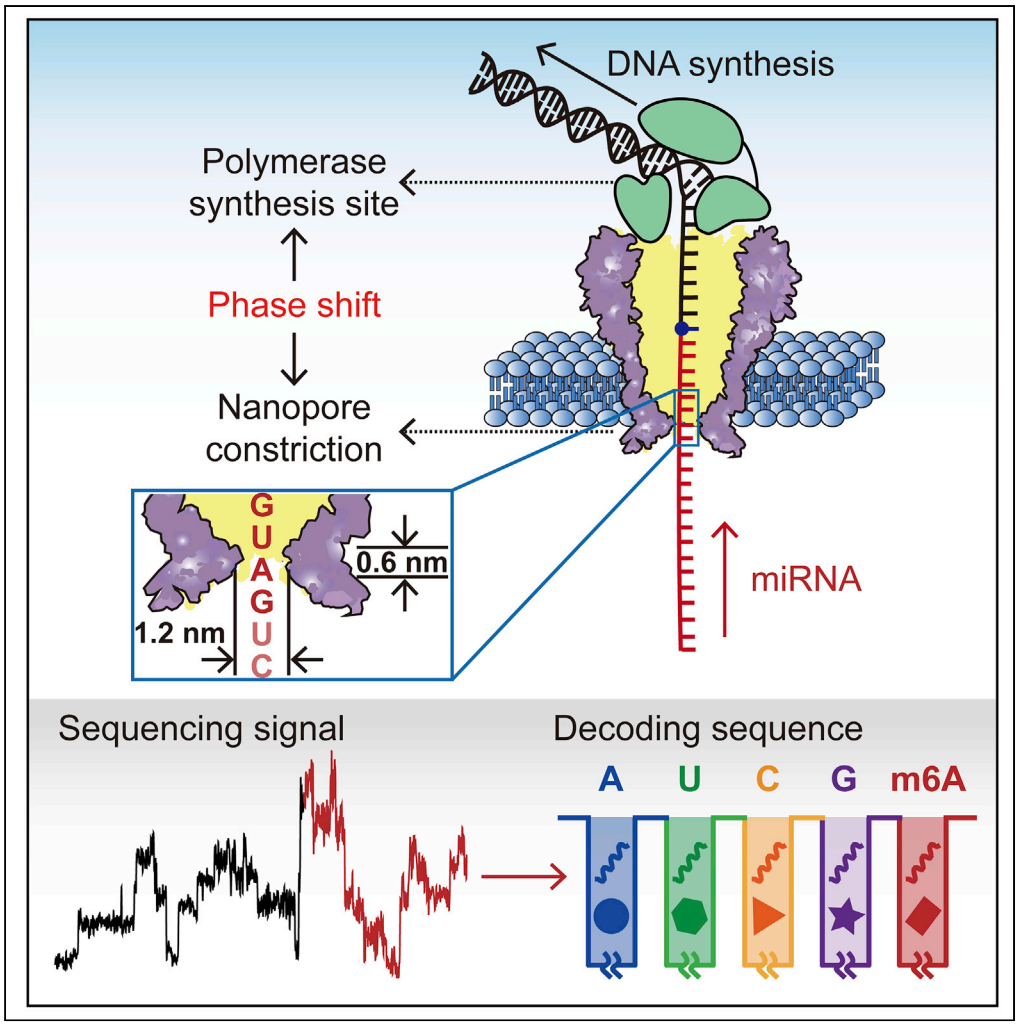

Jinyue Zhang, Shuanghong Yan, Le Chang, ..., Panke Zhang, Hong-Yuan Chen, Shuo Huang

shuo.huang@nju.edu.cn

HIGHLIGHTS

The first demonstration of single molecule miRNA sequencing

miRNA sequencing by NIPSS can directly identify epigenetic modifications

Enzymatic conjugation enables NIPSS sequencing of natural miRNAs

Zhang et al., iScience *23*, 100916
March 27, 2020
https://doi.org/10.1016/j.isci.2020.100916

iScience

CellPress

Article

Direct microRNA Sequencing Using Nanopore-Induced Phase-Shift Sequencing

Jinyue Zhang,[1,2,4] Shuanghong Yan,[1,2,4] Le Chang,[1,2] Weiming Guo,[1,2,3] Yuqin Wang,[1,2] Yu Wang,[1,2] Panke Zhang,[1,2] Hong-Yuan Chen,[1] and Shuo Huang[1,2,5,*]

SUMMARY

MicroRNAs (miRNAs) are a class of short non-coding RNAs that function in RNA silencing and post-transcriptional gene regulation. However, direct characterization of miRNA is challenging due to its unique properties such as its low abundance, sequence similarities, and short length. Although urgently needed, single molecule sequencing of miRNA has never been demonstrated, to the best of our knowledge. Nanopore-induced phase-shift sequencing (NIPSS), which is a variant form of nanopore sequencing, could directly sequence any short analytes including miRNA. In practice, NIPSS clearly discriminates between different identities, isoforms, and epigenetic variants of model miRNA sequences. This work thus demonstrates direct sequencing of miRNA, which serves as a complement to existing miRNA sensing routines by the introduction of the single molecule resolution. Future engineering of this technique may assist miRNA-based early stage diagnosis or inspire novel cancer therapeutics.

INTRODUCTION

MicroRNAs (miRNAs) are a group of short, single-stranded, non-coding RNAs that act as post-transcriptional gene regulators for a wide variety of physiological processes, including proliferation, differentiation, apoptosis, and immune reactions (Kim et al., 2018; Mehta and Baltimore, 2016). On the other hand, aberrant miRNA expression levels have been shown to be closely related to diverse diseases, such as cancer (Bracken et al., 2016; He et al., 2015; Nassar et al., 2017; Teng et al., 2017), auto-immune disorders (Pauley et al., 2009), and inflammatory diseases (Hatziapostolou et al., 2011).

MiRNAs function by binding to the 3′-untranslated region (3′UTR) of target messenger RNAs (Dong et al., 2013). Minor sequence variations, which include trimming, addition, or substitution of miRNA sequences, alter its binding affinities to target messenger RNA (Dong et al., 2013). As reported, miRNA isoforms (isomiRs) (Pritchard et al., 2012), which were generated by the addition or deletion of one or multiple nucleotides as terminal modifications, have been shown to participate in proliferative diseases (Boele et al., 2014) and cancer (Wu et al., 2015). On the other hand, N6-methyl-adenosine (m6A) modification, which serves as an RNA epigenetic marker (Niu et al., 2013) analogous to DNA methylation and histone modification (Liu and Pan, 2015), plays important roles in miRNA biogenesis (Alarcon et al., 2015; Berulava et al., 2015) and is related to the development of cancer (Konno et al., 2019). These functional roles of miRNAs are associated with their specific sequences and chemical modifications. However, it is a challenge to directly probe this information using existing tools for miRNA characterization.

Conventionally, miRNAs can be characterized by northern blot, quantitative reverse transcription polymerase chain reaction (qRT-PCR) assays or microarrays (Pritchard et al., 2012). Other emerging platforms for miRNA sensing include colorimetry (Wu et al., 2016), bioluminescence (Xu et al., 2017), enzymatic activity (Li et al., 2016), nanopore assays (Wang et al., 2011), and electrochemistry (Kilic et al., 2018). Unfortunately, these sensing methods provide limited analytical information because miRNA sequences are not directly reported and prior knowledge of the target miRNA sequence is required.

Next-generation sequencing (NGS) (Pritchard et al., 2012), which precisely identifies miRNAs without a prior need of its sequence information, is most widely used in miRNA investigations. However, existing approaches of miRNA sequencing by NGS are carried out by performing reverse transcription followed with deep sequencing of its complementary DNAs (cDNA) (Creighton et al., 2009), which suffers from unpredictable amplification biases and the loss of epigenetic information (Ozsolak and Milos, 2011; Pritchard et al., 2012). At present, there is no sequencing platforms that can directly and simultaneously report miRNA sequence and its base modifications along with a single molecule resolution.

[1]State Key Laboratory of Analytical Chemistry for Life Sciences, School of Chemistry and Chemical Engineering, Nanjing University, Nanjing 210023, China

[2]Chemistry and Biomedicine Innovation Center (ChemBIC), Nanjing University, Nanjing 210023, China

[3]Synthetic and Functional Biomolecules Center, Beijing National Laboratory for Molecular Sciences, Department of Chemical Biology, College of Chemistry and Molecular Engineering, Peking University, Beijing 100871, China

[4]These authors contributed equally

[5]Lead Contact

*Correspondence: shuo.huang@nju.edu.cn

https://doi.org/10.1016/j.isci.2020.100916

Recent developments in nanopore sequencing have demonstrated direct sequence readout from long stretches of DNA (Laszlo et al., 2014; Manrao et al., 2012) or RNA (Garalde et al., 2018) with a single molecule resolution and could directly resolve base modifications (Wang et al., 2019a; Wescoe et al., 2014). Presumably limited by the existing nanopore sequencing configuration and a lack of compatible motor proteins, direct sequencing of miRNAs and other short nucleic acid strands has unfortunately never been reported.

Nanopore-induced phase-shift sequencing (NIPSS) (Yan et al., 2019), which is a variant of nanopore sequencing, was recently developed as a universal strategy to sequence analytes other than long stretches of DNA (Laszlo et al., 2014) or RNA (Garalde et al., 2018), such as 2′-deoxy-2′-fluoroarabinonucleic acid (FANA) or other xeno nucleic acids (Yan et al., 2019). However, NIPSS is currently limited by a short read-length of ~15 nucleotides due to the length of the biological nanopore being used (Yan et al., 2019). Mature miRNAs, measuring ~22 nucleotides (nt) in length, are ideal analytes for NIPSS, even with its current configuration. Although the 15 nt read-length fails to cover the miRNA length completely, this technique is superior in principle to existing miRNA sensing methods because no amplification or prior knowledge of target sequences is required, whereas the epigenetic information within the sequence is still retained.

RESULTS AND DISCUSSION

Direct miRNA Sequencing Using NIPSS

To perform direct miRNA sequencing using NIPSS, the target miRNA strand must be conjugated with a section of DNA to form a DNA-miRNA chimeric template. In the eventual configuration, this chimera can be formed via chemical or enzymatic ligation, of which the miRNA section could be a strand of natural miRNA or its synthetic equivalent. However, to quickly prove this feasibility, this chimeric template, which is composed of a segment of DNA on the 3′-end and a segment of miRNA on the 5′-end with the two segments separated by an abasic spacer, was completely custom synthesized for a proof of concept demonstration (Figure 1A, Table S1). The abasic spacer serves to report a unique signal during NIPSS, indicating a clear transition from reading DNA to miRNA. The sequencing library was constructed by thermal annealing from three separate strands: the chimeric template, the primer, and the blocker (Figure 1A, Table S1, Transparent Methods) (Cherf et al., 2012; Yan et al., 2019).

NIPSS was carried out with a mutant *Mycobacterium smegmatis*porin A (MspA) nanopore (Transparent Methods), atop of which a wild-type (WT) phi29 DNA polymerase (DNAP) served as the ratcheting enzyme during sequencing (Yan et al., 2019). During NIPSS (Transparent Methods), the sequencing library, which is bound with the phi29 DNAP, was first electrophoretically dragged into the nanopore so that the blocker strand is mechanically unzipped. Subsequently, a phi29 DNAP-driven primer extension was initiated so that the chimeric template starts moving against the electrophoretic force in steps equivalent to a single nucleotide (Figure S1). The MspA nanopore reports a simultaneous reading of 4 nucleotides around the vicinity of its pore restriction.

As presented in Figure 1B, the DNA segment, the abasic spacer, and the miRNA segment sequentially pass through the nanopore constriction during NIPSS. The DNA segment thus acts as the "DNA drive strand." Utilizing the phase-shift between the polymerase synthesis site and the nanopore constriction, the phi29 DNAP enzymatically drives the DNA segment to move against the electrophoretic force and simultaneously the tethered miRNA segment is sequenced by the nanopore constriction. The DNA segment is designed to contain sequence repeats between "AAGA" and "TTTC" (3′–5′) to generate a unique signal pattern during NIPSS (Figure S2), which marks the initiation of a NIPSS event. The abasic spacer "X" following the DNA segment is expected to produce a high current signature that marks the initiation of miRNA sequencing within a NIPSS event (Figures S1 and S2, Table S1). Since this initiation, miRNA sequencing signals with a read-length of ~15 nucleotides are expected until the abasic spacer reaches the polymerase synthesis site (Yan et al., 2019). Unless otherwise stated, all NIPSS assays described in this paper were carried out by following this configuration. However, the miRNA segments from different chimeric templates contain varying sequences, whereas the DNA segment and the abasic spacer are kept unchanged (Table S1). It should be noted that even without the abasic spacer, we can still in principle discriminate miRNA signals during NIPSS. However, the placement of this abasic spacer serves as a clear signal marker, perfectly suited for a proof of concept demonstration for now.

Experimentally, miR-21, which is an intensively studied oncogenic miRNA and a cancer biomarker (Chan et al., 2005), was included in the miRNA segment of a chimeric strand (DNA-miR-21, Table S1) for

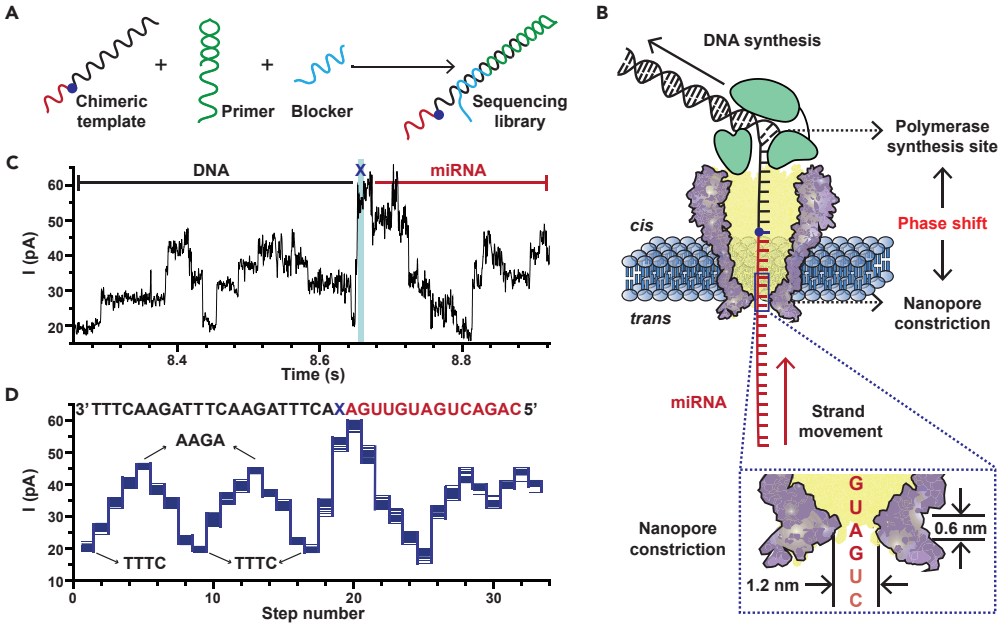

Figure 1. Direct miRNA Sequencing Using NIPSS

(A) A schematic diagram of the preparation of a sequencing library. The miRNA sequencing library is thermally annealed (Transparent Methods) from three separate nucleic acid strands, which include a chimeric template, a primer (green), and a blocker (light blue) (Table S1). The chimeric template is composed of a miRNA segment (red), an abasic residue (blue dot), and a DNA segment (black).

(B) The NIPSS strategy for direct miRNA sequencing. NIPSS is carried out with an MspA nanopore (purple) and a wild-type (WT) phi29 DNAP (green) by following the reported enzymatic ratcheting strategy (Figure S1) (Manrao et al., 2012). A fixed phase shift distance between the polymerase synthesis site and the pore constriction is utilized to directly sequence miRNA. During NIPSS, the DNA segment, the abasic residue, and the miRNA segment sequentially move through the nanopore constriction in single nucleotide steps until the abasic site (blue dot) reaches the binding pocket of phi29 DNAP. The inset image shows a zoomed-in view of the pore constriction. Due to the limited spatial resolution of the pore constriction, nanopore sequencing signals from MspA results from simultaneous reading of different combinations of sequence quadromers spanning the pore constriction during NIPSS.

(C) A typical current trace acquired by sequencing DNA-miR-21 (Table S1) using NIPSS. The DNA and miRNA segments of the trace are marked with black and red lines, respectively. The trace segment that corresponds to reading the abasic site (X) is marked with a blue stripe. Briefly, the DNA segment of the trace appears as two triangular shaped current characteristics due to the sequence design (Figure S2). The DNA segment of the trace is immediately followed by an abrupt increase of the signal due to the introduction of the abasic site after the DNA sequence. All step transitions after the abasic signal lead to miRNA sequencing signals.

(D) Overlay of multiple time-normalized events (N = 24) from the DNA-miR-21 results acquired by NIPSS. Each step in a sequencing event was extracted by a level detection algorithm (Transparent Methods, Figure S3). The corresponding sequence (3′-5′ convention, if not otherwise stated) is aligned above the statistics. The current levels of "AAGA" and "TTTC," which represents the highest and the lowest sequencing signals by reading the DNA part, are marked by black arrows. The demonstrated results were acquired by performing NIPSS with an aqueous buffer of 0.3 M KCl, 10 mM HEPES/KOH, 10 mM $MgCl_2$, 10 mM $(NH_4)_2SO_4$, and 4 mM DTT at pH 7.5.

See also Transparent Methods, Tables S1 and S2 and Figures S1–S4 and S11.

sequencing. A representative raw current trace of DNA-miR-21 is shown in Figure 1C. This trace can be segmented according to the characteristic sequencing pattern of the DNA drive strand and the abasic spacer respectively, from which the DNA segment reports two repeats of triangle-shaped signals and the abasic spacer reports an abnormally high step immediately after the signal from the DNA (Figure S2). Sequencing signals immediately subsequent from the abasic spacer report sequencing signals for miRNA. Specifically, the representative trace in Figure 1C reports sequencing signals from miR-21.

Mean current values of signal plateau during NIPSS were extracted from raw sequencing traces to form a squiggle plot (Transparent Methods, Figure S3), of which each step represents a simultaneous reading of four nucleotides. Here, the squiggle plot (van Dijk et al., 2018), which time-normalizes each signal plateau from raw sequencing traces, is useful in the demonstration of signal consistency between independent

events. Squiggle plots from 24 independent sequencing events acquired from DNA-miR-21 were overlapped in Figure 1D, from which the characteristic high and low current steps that correspond to nanopore readings of AAGA and TTTC were clearly recognized. After the signal from the abasic spacer, 14 subsequent steps that correspond to the sequence of miR-21 were demonstrated. Thus, direct miRNA sequencing by NIPSS has been conceptually demonstrated by sequencing a synthetic miR-21 moiety in the form of a DNA-miRNA chimera. NIPSS events from the same chimeric template demonstrate highly consistent nanopore sequencing patterns, which can be aligned with designed sequences.

The 2–8 nucleotides at the 5′ end of mature miRNAs serve as their seed sequence and normally report similar sequences among miRNAs from the same family, whereas miRNAs differ more significantly in sequence at their 3′-end. By analyzing all mature human miRNAs, as downloaded from the miRbase (http://www.mirbase.org/), it has been evidenced that ~99.5% of human miRNAs are in principle distinguishable by sequencing the first 15 nucleotides at their 3′-end (Figure S4, Table S2). These results indicate that NIPSS may already serve as a practical method for identifying other miRNAs, even with its current configuration.

Discrimination of miRNA Identities by NIPSS

Let-7a, which is a member of let-7 family miRNA (Pasquinelli et al., 2000), was included to form another chimeric template named DNA-let-7a for sequencing. Let-7 miRNA was the first human miRNA to have been discovered (Pasquinelli et al., 2000). In contrast to miR-21, which is a cancer biomarker, let-7 miRNA is known to target many oncogenes and thus it behaves as a cancer suppressor (Esquela-Kerscher and Slack, 2006). Simultaneous discrimination of miR-21 and let-7a, which are an oncogenic miRNA and a cancer suppressor miRNA respectively, thus shows significant bioanalytical value for cancer diagnosis and serves as an excellent example of miRNA identity recognition by NIPSS (Chen and Qin, 2011; Shishodia et al., 2015).

NIPSS sequencing of DNA-let-7a was carried out in a manner similar to that demonstrated in Figure 1. Representative raw sequencing data for DNA-miR-21 and DNA-let-7a are demonstrated in Figure S5. An overlay of squiggle plots from 24 independent DNA-miR-21 sequencing events (Figure 2A) and 12 independent DNA-let-7a sequencing events (Figure 2B) are summarized. The means and standard deviations from the extracted events in Figures 2A and 2B are shown together in Figure 2C. The sequencing steps from both chimeric templates show great alignment in the DNA part of the events. This is expected because the sequence of the DNA segment is identical in DNA-miR-21 and DNA-let-7a (Table S1). Starting from the steps of the abasic spacer however, the sequencing steps appear to deviate from one another due to sequence variations in their miRNA segments. Although preliminary, the observed variations of sequencing signals between let-7a and miR-21 support the hypothesis that different miRNA identities can be identified from an NIPSS assay.

To demonstrate that, a mixture of DNA-miR-21 and DNA-let-7a was subsequently sequenced using NIPSS. From measurements with the same nanopore, sequencing events of both chimeras were respectively observed, from which signatures of miR-21 or let-7a were quantitatively confirmed according to their signal variations from the aforementioned squiggle plot results when DNA-miR-21 or DNA-let-7a were respectively measured (Figure S6). This result thus successfully demonstrates that NIPSS is able to identify different miRNAs from their mixed form, especially when they show a major variation in their sequence, which is demonstrated with miR-21 and let-7a as a proof of concept.

Discriminating miRNA Isoforms by NIPSS

According to the scheme of direct miRNA sequencing by NIPSS, minor sequence variations such as addition, deletion, or substitution of nucleotides near the 3′-end of the target miRNA could in principle be resolved by resolution of a single nucleotide. Natural miRNA length isoforms (isomiRs), which result mainly from terminal additions or deletions of an indefinite number of nucleotides at the post-transcriptional level, differ at their 3′- or 5′-end in many mature miRNAs (Neilsen et al., 2012). IsomiRs have attracted significant attention due to their functional roles in diverse biological processes, which include modulation of miRNA stabilization (Boele et al., 2014), regulation of mRNA-targeting efficacy (Wu et al., 2015), and their correlations to different disease states (Boele et al., 2014; Kaushik et al., 2015; Pritchard et al., 2012; Wu et al., 2015). Most isomiRs differ by only a single nucleotide at either the 3′- or the 5′-end, such as mono-uridylation (Fei et al., 2018) or mono-adenylation (Thornton et al., 2014), and thus discrimination by conventional miRNA sensing routines is challenging. However, isomiRs differing at their 3′-ends as a result of non-template enzymatic additions (Koppers-Lalic et al., 2014) are more frequently observed and can be immediately distinguished with the current NIPSS scheme.

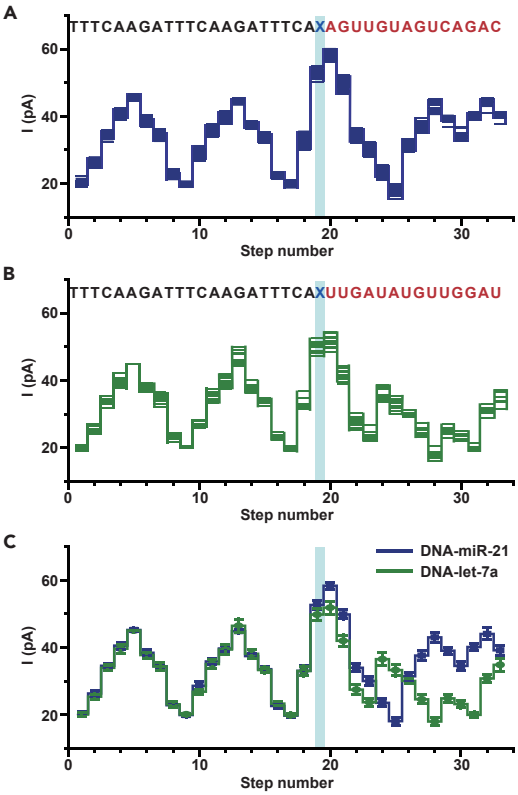

Figure 2. Identification of miRNAs Using NIPSS

Chimeric template strands containing miRNA-21 and Let-7a sequences were custom synthesized (Table S1) and directly sequenced by NIPSS.

(A) Overlay of multiple time-normalized events (N = 24) from the DNA-miR-21 results acquired by NIPSS.

(B) Overlay of multiple time-normalized events (N = 12) from the DNA-let-7a results acquired by NIPSS. (A, B) The corresponding sequences (DNA-miR-21 or DNA-Let-7a, 3′-5′ convention) are aligned above the plots. The DNA segments are marked in black and the miRNA segments are marked in red. The abasic site (X, blue), which separates the DNA and miRNA segments, acts as a signal marker to identify the sequence transition from reading DNA to miRNA during NIPSS.

(C) Consensus sequencing results in comparison between DNA-miR-21 and DNA-let-7a. The mean and standard deviation values are derived from time-normalized events, as demonstrated in A and B. The DNA part of the NIPSS results shows great alignment in all steps between both templates. However, the miRNA segment of the signals shows significant variations, starting from the step marked with the blue stripe. Blue stripes in (A–C) mark the sequencing step of TCAX, which is the first quadromer sequence containing the abasic residue when acquired by NIPSS.

See also Table S1, Figures S5 and S6.

The 3′ mono-uridylation product of miR-21, which is an isomiR of miR-21, is named miR-21 + U in this paper (Figure 3A). As reported, natural miR-21 + U isomiR is abundant in human urine samples and is a promising biomarker for prostate cancer (Koppers-Lalic et al., 2016). As a proof of concept, chimeric template DNA-miR-21 and DNA-miR-21 + U (Table S1) were designed and sequenced using the same NIPSS configuration (Figures 1 and 2). The means and standard deviations of extracted sequencing steps from 24 independent NIPSS events of DNA-miR-21 and DNA-miR-21 + U are shown in Figure 3B. As expected, the DNA segment of the NIPSS sequencing signal shows perfect alignment, because the DNA drive strands from both chimeric templates are identical in sequence. Distinct variation of the signal begins at step 23 as a consequence of the additional uridine at the 3′-end of miR-21 + U when compared with its isoform miR-21. Starting from step 23, all follow-up sequencing steps from miR-21 + U appear back shifted by 1 nucleotide (Figures 3B and 3C), which further confirms that the 3′uridylation isomiR has been recognized from direct NIPSS sequencing.

The demonstrated sequencing results between DNA-miR-21 and DNA-miR-21 + U have verified that isomiRs with minor sequence variations at the 3′-end can be clearly resolved using NIPSS. As demonstrated, addition or deletion of one or multiple nucleotides can be immediately detected from the characteristic signal variations and the subsequent pattern shift (Figure 3C). More representative data (Figure S7) and detailed statistics (Figure S8) are shown in the Supplemental Information. Minor sequence variations within the first 14 nucleotides to the 3′-end of the target miRNAs can be discriminated by following the same strategy. This makes direct miRNA sequencing by NIPSS immediately applicable to the discrimination between miRNAs from the same family, which share the same 5′ terminal seed sequences but show subtle variations in the sequence region to their 3′-end (Brancati and Groβhans, 2018; Moore et al., 2015).

Detecting m6A Modification within miRNA

RNA modifications represent a type of epigenetic regulation of gene expression (Lence et al., 2016; Liu and Pan, 2015), of which N6-methyladenosine (m6A) is the most abundant modifications (Lence et al., 2016; Liu and Pan, 2015; Niu et al., 2013). The reversible m6A modification is recognized as a novel epigenetic marker

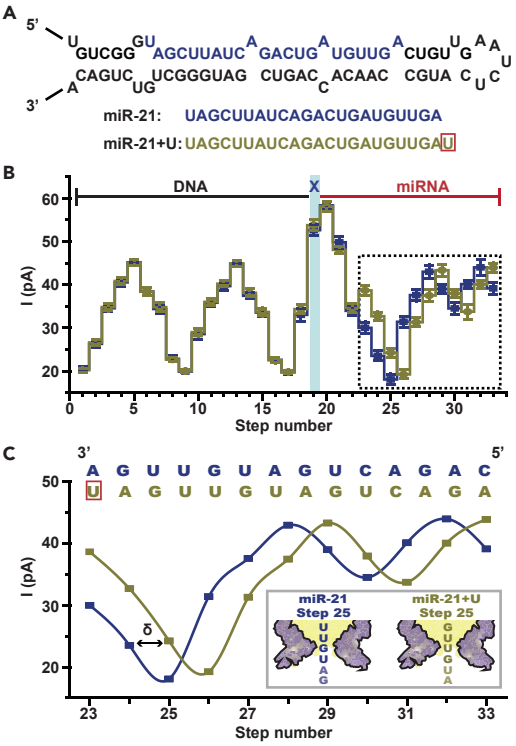

Figure 3. Discrimination of miRNA Isoforms (isomiRs) Using NIPSS

(A) miR-21 and its isoforms. The upper image demonstrates the structure of a precursor microRNA (pre-miRNA) for human miR-21. The lower image demonstrates the sequence (5′-3′) of mature miR-21 and its miR-21 + U isoform, respectively. An additional uracil (red box) exists at the 3′-end of miR-21 + U.

(B) Comparison of consensus sequencing results between DNA-miR-21 and DNA-miR-21 + U. The means and standard deviations were derived from 24 time-normalized independent events for DNA-miR-21 (blue) and DNA-miR-21 + U (brown) respectivly (Table S3). The DNA, the abasic site, and the miRNA part of the signal are marked separately. The blue strip marks the sequencing step of TCAX, which is the first sequence quadromer containing an abasic spacer encountered by NIPSS. The demonstrated statistical results show great alignment in all parts except that marked with a dashed-line box.

(C) Sequencing result shift between DNA-miR-21 and DNA-miR-21 + U. A zoomed-in view of the dashed-line box in B illustrates a shift effect of current levels caused by a nucleotide insertion of DNA-miR-21 + U in reference to DNA-miR-21. The aligned sequence context above the results demonstrates that the addition of a uracil (red box) in DNA-miR-21 + U systematically generates 1 nucleotide (marked as δ) shift. This single nucleotide result shift is also demonstrated by the schematic diagram in the image inset, which takes the results of step 25 as an example. See also Tables S1 and S3, Figures S7 and S8.

that plays a critical role in mRNA metabolism (Dai et al., 2018), cellular functions (Lence et al., 2016; Roundtree et al., 2017; Zhao et al., 2017), and miRNA biogenesis (Alarcon et al., 2015; Berulava et al., 2015). Recent studies reveal that m6A also exist in mature miRNAs (Berulava et al., 2015; Konno et al., 2019), and their aberrant level of existence is related to gastrointestinal cancers (Konno et al., 2019). However, due to the chemical and biochemical similarities between adenosine and m6A, precise localization of m6A modifications from natural miRNAs becomes technically challenging for any next-generation sequencing platform. The emergence of the technique of MeRIP-seq (methylated RNA immunoprecipitation followed by sequencing) (Dominissini et al., 2012; Meyer et al., 2012) is a major advance for this technical need. However, MeRIP-seq still requires reverse transcription followed by amplification and fails to achieve single nucleotide resolution. Recent developments of direct RNA sequencing using nanopores have successfully demonstrated m6A mapping directly from mRNA samples (Garalde et al., 2018). However, direct RNA sequencing by nanopores is only applicable to sequencing long stretches of RNA instead of miRNAs, whereas MeRIP-seq fails to achieve single molecule and single nucleotide resolutions.

NIPSS is particularly useful in distinguishing minor sequence variations approaching the 3′-end of the target miRNAs. To verify whether single m6A modification within a short stretch of miRNA could be identified by NIPSS, a conceptual experiment was designed. The first nucleotide at the 3′-end of the miRNA segment of DNA-miR-21 is changed from a canonical adenosine to m6A (Figure 4A). This new strand is named as DNA-miR-21 (m6A) and is custom synthesized for downstream NIPSS characterization. According to the NIPSS convention, the m6A reaches the pore constriction first (Figure 4B), which makes this nucleotide highly resolvable by the current NIPSS configuration and thus becomes an optimum option for a proof-of-concept demonstration.

Representative NIPSS sequencing traces from DNA-miR-21 (Figure 4C) and DNA-miR-21(m6A) (Figure 4D) show noticeable differences in the current height of the sequencing steps, which correspond to the first nucleotide at the 3′-end of the miRNA segment. For a zoomed-in demonstration, only the fraction of the sequencing traces that correspond to the region of interest is shown (Figures 4C and 4D), and the

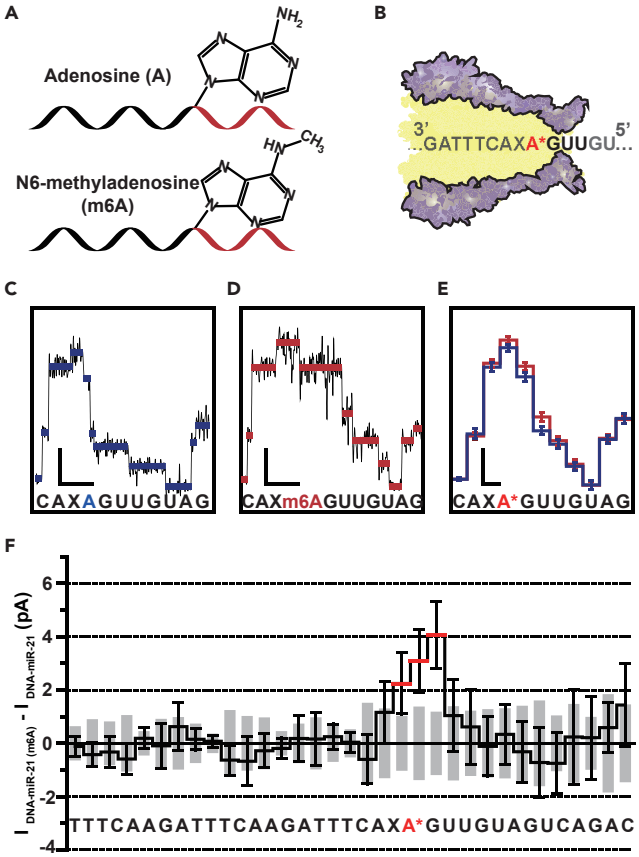

Figure 4. Direct N6-methyladenosine (m6A) Mapping Using NIPSS

(A) Schematic diagram of chimeric template strands containing canonical adenosine (A) or N6-methyladenosine (m6A). A single "A" or "m6A" is embedded in different chimeric strands (top: DNA-miR-21, bottom: DNA-miR-21(m6A), Table S1) for NIPSS sequencing, where its chemical structure and location is annotated. Black and red segments represent the DNA and the miRNA part of the strand.

(B) Schematic diagram of NIPSS sequencing of miRNA containing "A" or "m6A" nucleotides. A* within the sequence context represents the "A" or "m6A" nucleotide within the strand.

(C) A representative current trace of DNA-miR-21 sequenced by NIPSS. Blue lines represent extracted mean current values from each step. The corresponding sequence context is aligned below in which a canonical adenosine is marked in blue.

(D) A representative current trace when DNA-miR-21(m6A) is sequenced by NIPSS. Red lines represent extracted mean current values from each step. The corresponding sequence context is aligned below, from which a N6-methyladenosine is marked in red. Scale bars in C and D represents 10 pA (current, vertical) and 50 ms (time, horizontal), respectively.

(E) Consensus sequencing results in comparison between DNA-miR-21 and DNA-miR-21(m6A). The means and standard deviations were derived from 24 independent events. A* within the sequence context below the results represents either A or m6A.

(F) Current differences between NIPSS results of DNA-miR-21 and DNA-miR-21(m6A). These differences were derived by calculating $\Delta I = I_{DNA-miR-21(m6A)} - I_{DNA-miR-21}$ from the mean values of 24 events from each strand, with the associated sequence aligned below. The standard deviation values of DNA-miR-21 are demonstrated with gray column, and the standard deviation of DNA-miR-21(m6A) is demonstrated with black error bars. The m6A modification results in a signal variation when m6A containing sequence quadromers were read by the nanopore constriction. Due to the limited spatial resolution of MspA, a single m6A modification results in detectable signal fluctuations within three current steps as marked by red lines.

See also Table S1, Figures S9 and S10.

additional raw sequencing events are illustrated in Figure S9. The means and standard deviations of the extracted current steps of 24 independent NIPSS events from DNA-miR-21 (blue) and DNA-miR-21(m6A) (red) are summarized and superimposed in Figure 4E. Due to the limited spatial resolution of the MspA constriction, ~3 steps show significant signal variations between the two analytes due to the introduced

m6A modification, whereas other sequencing steps show a clear alignment, as the remainder of the sequence is identical. The difference of sequencing step heights between DNA-miR-21 (m6A) and DNA-miR-21 are shown in Figure 4F, from which the maximum signal variation between the two analytes could achieve a difference of ~4 pA in the corresponding positions of the signals, due to the introduced chemical modification (Figure S10).

Library Preparation by Enzymatic Conjugation

To sequence miRNAs from natural resources by NIPSS, the target miRNA strands must be conjugated chemically or enzymatically with the DNA drive-strand ahead of the library preparation. An enzymatic ligation strategy has been reported (Lee and Yi, 2014) and could be adapted for this purpose.

Briefly, the 5′ phosphorylated DNA drive strand ($5PO_4$ DNA) is first treated with a 5′ DNA adenylation kit (New England Biolabs), assisted with the Mth RNA ligase (Figure S11). The adenylated DNA drive strand (5AppDNA) was characterized and purified by ethanol precipitation and further ligated to the 3′-end of the target miRNA strands by the T4 RNA ligase 2 truncated K227Q mutant (T4 Rnl2tr). After this ligation, the DNA-miRNA chimeric template can be characterized by electrophoresis on a 15% polyacrylamide gel, and the ligated chimeric template is shown as the extra band of higher molecular weight (Figure S11).

We then performed NIPSS to sequence these enzymatically ligated chimeric strands. As shown in Figure S12, sequencing signals from the synthetic and the ligated chimera show strong resemblance in their signal patterns. The means and standard deviations of sequencing steps were extracted from more than 20 independent events from each analyte. These results confirmed that the above demonstrated NIPSS strategy could be applied to sequence miRNAs from natural sources with a current demonstration using their synthetic equivalent.

Conclusion

In summary, we demonstrate single molecule sequencing of miRNA, using an NIPSS approach. Similar strategies could also be adapted to sequence other short non-coding strands, such as siRNA (Bernstein et al., 2001) or piRNA (Siomi et al., 2011), avoiding the laborious motor protein engineering for nanopore sequencing (Garalde et al., 2018). Although demonstrated as a prototype, the NIPSS results in this paper show clear signal discriminations between different sequences, isoforms, and epigenetic modifications among synthetic miRNA sequences. MiRNAs from natural resources, such as miRNA extracts from clinical samples, can be conjugated with pre-designed DNA linker strands by performing routine enzymatic ligation to build NIPSS sequencing libraries (Figure S13). Consequently, direct miRNA sequencing by NIPSS could be directly implemented in clinical diagnosis or could be utilized as a complement to existing miRNA sensing platforms when single-base resolution becomes critical. MiRNA sequencing by NIPSS shares the same advantages of other nanopore sequencing technologies, including low-cost, single-base resolution and portability. In principle, NIPSS, when properly engineered, could also be adapted to commercial nanopore sequencers, such as MinION™ (Oxford Nanopore Technologies, UK) (Garalde et al., 2018). However, direct miRNA sequencing has not been demonstrated by Oxford Nanopore Technologies, likely due to the short length of a miRNA strand or its incompatibility with the helicase motor protein. Ultimately, high-throughput direct miRNA sequencing by NIPSS can be carried out in optical nanopore chips (Huang et al., 2015; Wang et al., 2019b) for low-cost, high-throughput, and multiplexed miRNA characterizations in a disposable device form.

Limitations of the Study

MiRNA sequencing by NIPSS is currently limited to sequence the first 14-15 nucleotides to the 3′-end of any miRNA types. To further extend the read-length of NIPSS to the full length of miRNA, an engineered MspA or phi29 DNAP with redundant structures could be constructed to extend the phase-shift distance of NIPSS. Alternatively, existing nanopores of larger dimensions such as ClyA (Soskine et al., 2012) and FraC (Huang et al., 2017) may be adapted to sequence full-length miRNA in its precursor or primary form. Chemical ligations (Paredes et al., 2011; Vogel and Richert, 2012) between the 5′-end of target miRNAs and the 5′-end of the DNA drive strand may be carried out to form a reverse chimeric strand with a "head to head" configuration for 5′-end miRNA sequencing by NIPSS.

METHODS

All methods can be found in the accompanying Transparent Methods supplemental file.

SUPPLEMENTAL INFORMATION

Supplemental Information can be found online at https://doi.org/10.1016/j.isci.2020.100916.

ACKNOWLEDGMENTS

This project was funded by National Natural Science Foundation of China (No. 91753108, No. 21675083, No. 31972917), Fundamental Research Funds for the Central Universities (No. 020514380174, No. 020514380142), State Key Laboratory of Analytical Chemistry for Life Sciences (No. 5431ZZXM1902, No. 5431ZZXM1804), 1000 Plan Youth Talent Program of China, Programs for high-level entrepreneurial and innovative talents introduction of Jiangsu Province, Technology innovation fund program of Nanjing University, and Excellent Research Program of Nanjing University (Grant No.ZYJH004).

AUTHOR CONTRIBUTIONS

J.Y.Z. and S.H. conceived the project design. J.Y.Z performed the experiments. S.H.Y. prepared the MspA nanopore. Y.W. designed the DNA sequences. L.C., W.M.G., Y.W., J.Y.Z., and S.H. analyzed the data. Y.Q.W., P.K.Z., and S.H.Y. set up the instruments. S.H. and J.Y.Z. wrote the paper. S.H. and H.Y.C. supervised the project.

DECLARATION OF INTERESTS

S.H., J.Y.Z., and S.H.Y. are inventors on a filed PCT patent application related to this work (PCT/CN2019/102162, Aug/23/2019). The authors declare no other competing interests.

Received: January 15, 2020
Revised: January 31, 2020
Accepted: February 11, 2020
Published: March 27, 2020

REFERENCES

Alarcon, C.R., Lee, H., Goodarzi, H., Halberg, N., and Tavazoie, S.F. (2015). N6-methyladenosine marks primary microRNAs for processing. Nature *519*, 482–485.

Bernstein, E., Caudy, A.A., Hammond, S.M., and Hannon, G.J. (2001). Role for a bidentateribonuclease in the initiation step of RNA interference. Nature *409*, 363–366.

Berulava, T., Rahmann, S., Rademacher, K., Klein-Hitpass, L., and Horsthemke, B. (2015). N6-adenosine methylation in MiRNAs. PLoS One *10*, e0118438.

Boele, J., Persson, H., Shin, J.W., Ishizu, Y., Newie, I.S., Sokilde, R., Hawkins, S.M., Coarfa, C., Ikeda, K., Takayama, K., et al. (2014). PAPD5-mediated 3′ adenylation and subsequent degradation of miR-21 is disrupted in proliferative disease. Proc Natl Acad Sci U S A *111*, 11467–11472.

Bracken, C.P., Scott, H.S., and Goodall, G.J. (2016). A network-biology perspective of microRNA function and dysfunction in cancer. Nat. Rev. Genet. *17*, 719–732.

Brancati, G., and Großhans, H. (2018). An interplay of miRNA abundance and target site architecture determines miRNA activity and specificity. Nucleic Acids Res. *46*, 3259–3269.

Chan, J.A., Krichevsky, A.M., and Kosik, K.S. (2005). MicroRNA-21 is an antiapoptotic factor in human glioblastoma cells. Cancer Res. *65*, 6029–6033.

Chen, X., and Qin, Z. (2011). Post-transcriptional regulation by microrna-21 and let-7a microRNA in paediatriccholesteatoma. J. Int. Med. Res. *39*, 2110–2118.

Cherf, G.M., Lieberman, K.R., Rashid, H., Lam, C.E., Karplus, K., and Akeson, M. (2012). Automated forward and reverse ratcheting of DNA in a nanopore at 5-A precision. Nat. Biotechnol. *30*, 344–348.

Creighton, C.J., Reid, J.G., and Gunaratne, P.H. (2009). Expression profiling of microRNAs by deep sequencing. Brief. Bioinform. *10*, 490–497.

Dai, D., Wang, H., Zhu, L., Jin, H., and Wang, X. (2018). N6-methyladenosine links RNA metabolism to cancer progression. Cell Death Dis. *9*, 124.

Dominissini, D., Moshitch-Moshkovitz, S., Schwartz, S., Salmon-Divon, M., Ungar, L., Osenberg, S., Cesarkas, K., Jacob-Hirsch, J., Amariglio, N., Kupiec, M., et al. (2012). Topology of the human and mouse m6A RNA methylomes revealed by m6A-seq. Nature *485*, 201–206.

Dong, H., Lei, J., Ding, L., Wen, Y., Ju, H., and Zhang, X. (2013). MicroRNA: function, detection, and bioanalysis. Chem. Rev. *113*, 6207–6233.

Esquela-Kerscher, A., and Slack, F.J. (2006). Oncomirs—microRNAs with a role in cancer. Nat. Rev. Cancer *6*, 259–269.

Fei, Q., Yu, Y., Liu, L., Zhang, Y., Baldrich, P., Dai, Q., Chen, X., and Meyers, B.C. (2018). Biogenesis of a 22-nt microRNA in Phaseoleae species by precursor-programmed uridylation. Proc Natl Acad Sci U S A *115*, 8037–8042.

Garalde, D.R., Snell, E.A., Jachimowicz, D., Sipos, B., Lloyd, J.H., Bruce, M., Pantic, N., Admassu, T., James, P., Warland, A., et al. (2018). Highly parallel direct RNA sequencing on an array of nanopores. Nat. Methods *15*, 201–206.

Hatziapostolou, M., Polytarchou, C., Aggelidou, E., Drakaki, A., Poultsides, G.A., Jaeger, S.A., Ogata, H., Karin, M., Struhl, K., Hadzopoulou-Cladaras, M., et al. (2011). An HNF4α-miRNA inflammatory feedback circuit regulates hepatocellular oncogenesis. Cell *147*, 1233–1247.

He, Y., Lin, J., Kong, D., Huang, M., Xu, C., Kim, T.K., Etheridge, A., Luo, Y., Ding, Y., and Wang, K. (2015). Current state of circulating MicroRNAs as cancer biomarkers. Clin. Chem. *61*, 1138–1155.

Huang, S., Romero-Ruiz, M., Castell, O.K., Bayley, H., and Wallace, M.I. (2015). High-throughput optical sensing of nucleic acids in a nanopore array. Nat. Nanotechnol. *10*, 986–991.

Huang, G., Willems, K., Soskine, M., Wloka, C., and Maglia, G. (2017). Electro-osmotic capture and ionic discrimination of peptide and protein biomarkers with FraC nanopores. Nat. Commun. *8*, 935.

Kaushik, A., Saraf, S., Mukherjee, S.K., and Gupta, D. (2015). miRMOD: a tool for identification and analysis of 5′ and 3′ miRNA modifications in Next Generation Sequencing small RNA data. PeerJ *3*, e1332.

Kilic, T., Erdem, A., Ozsoz, M., and Carrara, S. (2018). microRNA biosensors: opportunities and challenges among conventional and commercially available techniques. Biosens. Bioelectron. *99*, 525–546.

Kim, J., Yao, F., Xiao, Z., Sun, Y., and Ma, L. (2018). MicroRNAs and metastasis: small RNAs play big roles. Cancer Metastasis Rev. *37*, 5–15.

Konno, M., Koseki, J., Asai, A., Yamagata, A., Shimamura, T., Motooka, D., Okuzaki, D., Kawamoto, K., Mizushima, T., and Eguchi, H. (2019). Distinct methylation levels of mature microRNAs in gastrointestinal cancers. Nat. Commun. *10*, 3888.

Koppers-Lalic, D., Hackenberg, M., Bijnsdorp, I.V., van Eijndhoven, M.A.J., Sadek, P., Sie, D., Zini, N., Middeldorp, J.M., Ylstra, B., de Menezes, R.X., et al. (2014). Nontemplated nucleotide additions distinguish the small RNA composition in cells from exosomes. Cell Rep. *8*, 1649–1658.

Koppers-Lalic, D., Hackenberg, M., De Menezes, R., Misovic, B., Wachalska, M., Geldof, A., Zini, N., De Reijke, T., Wurdinger, T., and Vis, A.J.O. (2016). Non-invasive prostate cancer detection by measuring miRNA variants (isomiRs) in urine extracellular vesicles. Oncotarget *7*, 22566–22578.

Laszlo, A.H., Derrington, I.M., Ross, B.C., Brinkerhoff, H., Adey, A., Nova, I.C., Craig, J.M., Langford, K.W., Samson, J.M., Daza, R., et al. (2014). Decoding long nanopore sequencing reads of natural DNA. Nat. Biotechnol. *32*, 829–833.

Lee, J.E., and Yi, R. (2014). Highly efficient ligation of small RNA molecules for microRNA quantitation by high-throughput sequencing. J. Vis. Exp. *93*, e52095.

Lence, T., Akhtar, J., Bayer, M., Schmid, K., Spindler, L., Ho, C.H., Kreim, N., Andrade-Navarro, M.A., Poeck, B., Helm, M., et al. (2016). m(6)A modulates neuronal functions and sex determination in Drosophila. Nature *540*, 242–247.

Li, B., Liu, F., Peng, Y., Zhou, Y., Fan, W., Yin, H., Ai, S., and Zhang, X. (2016). Two-stage cyclic enzymatic amplification method for ultrasensitive electrochemical assay of microRNA-21 in the blood serum of gastric cancer patients. Biosens. Bioelectron. *79*, 307–312.

Liu, N., and Pan, T. (2015). RNA epigenetics. Transl. Res. *165*, 28–35.

Manrao, E.A., Derrington, I.M., Laszlo, A.H., Langford, K.W., Hopper, M.K., Gillgren, N., Pavlenok, M., Niederweis, M., and Gundlach, J.H. (2012). Reading DNA at single-nucleotide resolution with a mutant MspA nanopore and phi29 DNA polymerase. Nat. Biotechnol. *30*, 349–353.

Mehta, A., and Baltimore, D. (2016). MicroRNAs as regulatory elements in immune system logic. Nat. Rev. Immunol. *16*, 279–294.

Meyer, K.D., Saletore, Y., Zumbo, P., Elemento, O., Mason, C.E., and Jaffrey, S.R. (2012). Comprehensive analysis of mRNA methylation reveals enrichment in 3′ UTRs and near stop codons. Cell *149*, 1635–1646.

Moore, M.J., Scheel, T.K., Luna, J.M., Park, C.Y., Fak, J.J., Nishiuchi, E., Rice, C.M., and Darnell, R.B. (2015). miRNA–target chimeras reveal miRNA 3′-end pairing as a major determinant of Argonaute target specificity. Nat. Commun. *6*, 8864.

Nassar, F.J., Nasr, R., and Talhouk, R. (2017). MicroRNAs as biomarkers for early breast cancer diagnosis, prognosis and therapy prediction. Pharmacol. Ther. *172*, 34–49.

Neilsen, C.T., Goodall, G.J., and Bracken, C.P. (2012). IsomiRs–the overlooked repertoire in the dynamic microRNAome. Trends Genet. *28*, 544–549.

Niu, Y., Zhao, X., Wu, Y.S., Li, M.M., Wang, X.J., and Yang, Y.G. (2013). N6-methyl-adenosine (m6A) in RNA: an old modification with a novel epigenetic function. Genomics Proteomics Bioinformatics *11*, 8–17.

Ozsolak, F., and Milos, P.M. (2011). RNA sequencing: advances, challenges and opportunities. Nat. Rev. Genet. *12*, 87–98.

Paredes, E., Evans, M., and Das, S.R. (2011). RNA labeling, conjugation and ligation. Methods *54*, 251–259.

Pasquinelli, A.E., Reinhart, B.J., Slack, F., Martindale, M.Q., Kuroda, M.I., Maller, B., Hayward, D.C., Ball, E.E., Degnan, B., Müller, P., et al. (2000). Conservation of the sequence and temporal expression of let-7 heterochronic regulatory RNA. Nature *408*, 86–89.

Pauley, K.M., Cha, S., and Chan, E.K. (2009). MicroRNA in autoimmunity and autoimmune diseases. J. Autoimmun. *32*, 189–194.

Pritchard, C.C., Cheng, H.H., and Tewari, M. (2012). MicroRNA profiling: approaches and considerations. Nat. Rev. Genet. *13*, 358–369.

Roundtree, I.A., Evans, M.E., Pan, T., and He, C. (2017). Dynamic RNA modifications in gene expression regulation. Cell *169*, 1187–1200.

Shishodia, G., Shukla, S., Srivastava, Y., Masaldan, S., Mehta, S., Bhambhani, S., Sharma, S., Mehrotra, R., Das, B.C., and Bharti, A.C. (2015). Alterations in microRNAs miR-21 and let-7a correlate with aberrant STAT3 signaling and downstream effects during cervical carcinogenesis. Mol. Cancer *14*, 116.

Siomi, M.C., Sato, K., Pezic, D., and Aravin, A.A. (2011). PIWI-interacting small RNAs: the vanguard of genome defence. Nat. Rev. Mol. Cell Biol. *12*, 246–258.

Soskine, M., Biesemans, A., Moeyaert, B., Cheley, S., Bayley, H., and Maglia, G. (2012). An engineered ClyA nanopore detects folded target proteins by selective external association and pore entry. Nano Lett. *12*, 4895–4900.

Teng, Y., Ren, Y., Hu, X., Mu, J., Samykutty, A., Zhuang, X., Deng, Z., Kumar, A., Zhang, L., Merchant, M.L., et al. (2017). MVP-mediated exosomal sorting of miR-193a promotes colon cancer progression. Nat. Commun. *8*, 14448.

Thornton, J.E., Du, P., Jing, L., Sjekloca, L., Lin, S., Grossi, E., Sliz, P., Zon, L.I., and Gregory, R.I. (2014). Selective microRNA uridylation by Zcchc6 (TUT7) and Zcchc11 (TUT4). Nucleic Acids Res. *42*, 11777–11791.

van Dijk, E.L., Jaszczyszyn, Y., Naquin, D., and Thermes, C. (2018). The third revolution in sequencing technology. Trends Genet. *34*, 666–681.

Vogel, H., and Richert, C. (2012). Labeling small RNAs through chemical ligation at the 5′ terminus: enzyme-free or combined with enzymatic 3′-labeling. Chembiochem *13*, 1474–1482.

Wang, Y., Patil, K.M., Yan, S., Zhang, P., Guo, W., Wang, Y., Chen, H.Y., Gillingham, D., and Huang, S. (2019a). Nanopore sequencing accurately identifies the mutagenic DNA lesion O6-carboxymethyl guanine and reveals its behavior in replication. Angew.Chem. Int. Ed. *58*, 8432–8436.

Wang, Y., Wang, Y., Du, X., Yan, S., Zhang, P., Chen, H.-Y., and Huang, S. (2019b). Electrode-free nanopore sensing by DiffusiOptoPhysiology. Sci. Adv. *5*, eaar3309.

Wang, Y., Zheng, D., Tan, Q., Wang, M.X., and Gu, L.Q. (2011). Nanopore-based detection of circulating microRNAs in lung cancer patients. Nat. Nanotechnol. *6*, 668–674.

Wescoe, Z.L., Schreiber, J., and Akeson, M. (2014). Nanopores discriminate among five C5-cytosine variants in DNA. J. Am. Chem. Soc. *136*, 16582–16587.

Wu, H., Liu, Y., Wang, H., Wu, J., Zhu, F., and Zou, P. (2016). Label-free and enzyme-free colorimetric detection of microRNA by catalyzed hairpin assembly coupled with hybridization chain reaction. Biosens. Bioelectron. *81*, 303–308.

Wu, X., Zeng, R., Wu, S., Zhong, J., Yang, L., and Xu, J. (2015). Comprehensive expression analysis of miRNA in breast cancer at the miRNA and isomiR levels. Gene *557*, 195–200.

Xu, Q., Ma, F., Huang, S.Q., Tang, B., and Zhang, C.Y. (2017). Nucleic acid amplification-free bioluminescent detection of MicroRNAs with high sensitivity and accuracy based on controlled target degradation. Anal. Chem. *89*, 7077–7083.

Yan, S., Li, X., Zhang, P., Wang, Y., Chen, H.Y., Huang, S., and Yu, H. (2019). Direct sequencing of 2′-deoxy-2′-fluoroarabinonucleic acid (FANA) using nanopore-induced phase-shift sequencing (NIPSS). Chem. Sci. *10*, 3110–3117.

Zhao, B.S., Roundtree, I.A., and He, C. (2017). Post-transcriptional gene regulation by mRNA modifications. Nat. Rev. Mol. Cell Biol. *18*, 31–42.

iScience, Volume *23*

Supplemental Information

Direct microRNA Sequencing Using Nanopore-Induced Phase-Shift Sequencing

Jinyue Zhang, Shuanghong Yan, Le Chang, Weiming Guo, Yuqin Wang, Yu Wang, Panke Zhang, Hong-Yuan Chen, and Shuo Huang

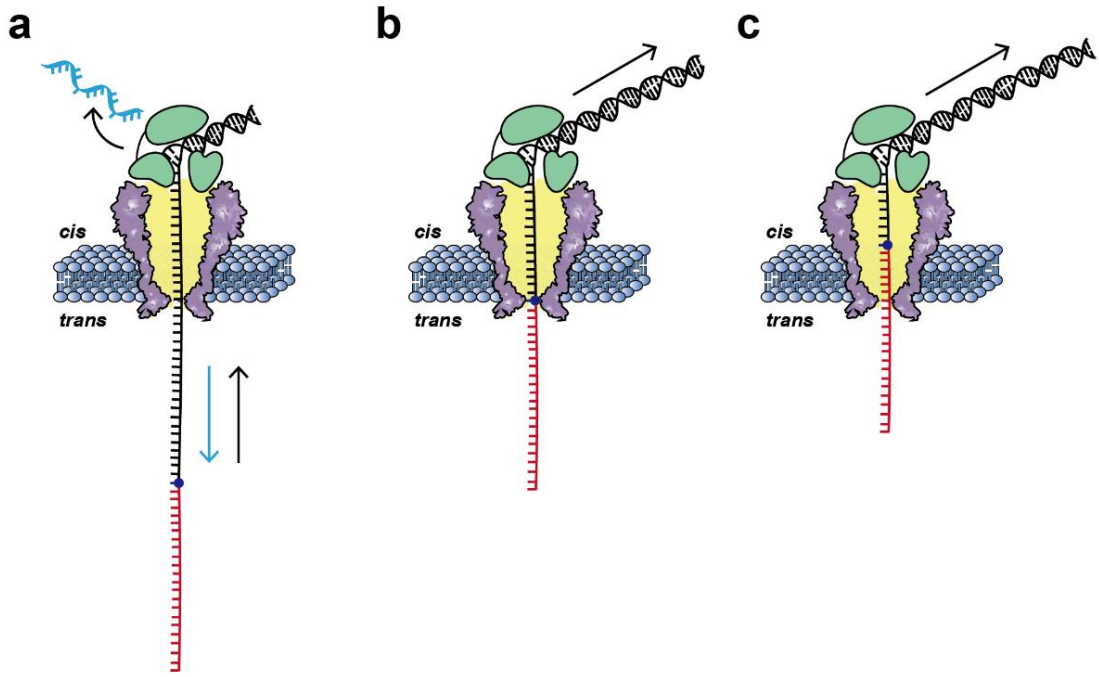

Figure S1: Detailed schematic diagrams of NIPSS, Related to Figure 1. The configuration of direct miRNA sequencing by NIPSS is as reported previously (Yan et al., 2019). The chimeric template is composed of a miRNA segment (red), an abasic residue (blue dot) and a DNA segment (black) **(Methods 1)**. With a +180 mV applied potential, the sequencing library, which was bound with a phi29 DNAP (green), was driven electrophoretically into the MspA nanopore (purple). **a)** The initiation of NIPSS. The cyan DNA blocker strand, which was thermally annealed with the sequencing library, was first voltage-driven unzipped from the chimeric template. This unzipping consequently triggered the replication-driven ratcheting by the phi29 DNA polymerase on top of the nanopore. The transition from voltage-driven unzipping to replication-driven ratcheting represents the initiation of nanopore sequencing. The motion directions of the chimeric template during unzipping and ratcheting are marked with cyan and black arrows, respectively. **b)** The initiation of miRNA sequencing. Passage of the abasic spacer through the pore constriction marks the initiation of subsequent miRNA sequencing. **c)** MiRNA sequencing by NIPSS. By utilizing the phase-shift, the miRNA segment passes through the pore constriction with single nucleotide steps, when the DNA drive-strand is being replicated by the phi29 DNA polymerase. All NIPSS experiments in this paper follow this configuration. All sequencing experiments were performed at 23 ^{o}C in the sequencing buffer of 0.3 M KCl, 10 mM HEPES/KOH, 10 mM $MgCl_2$, 10 mM $(NH_4)_2SO_4$ and 4 mM DTT at pH 7.5.

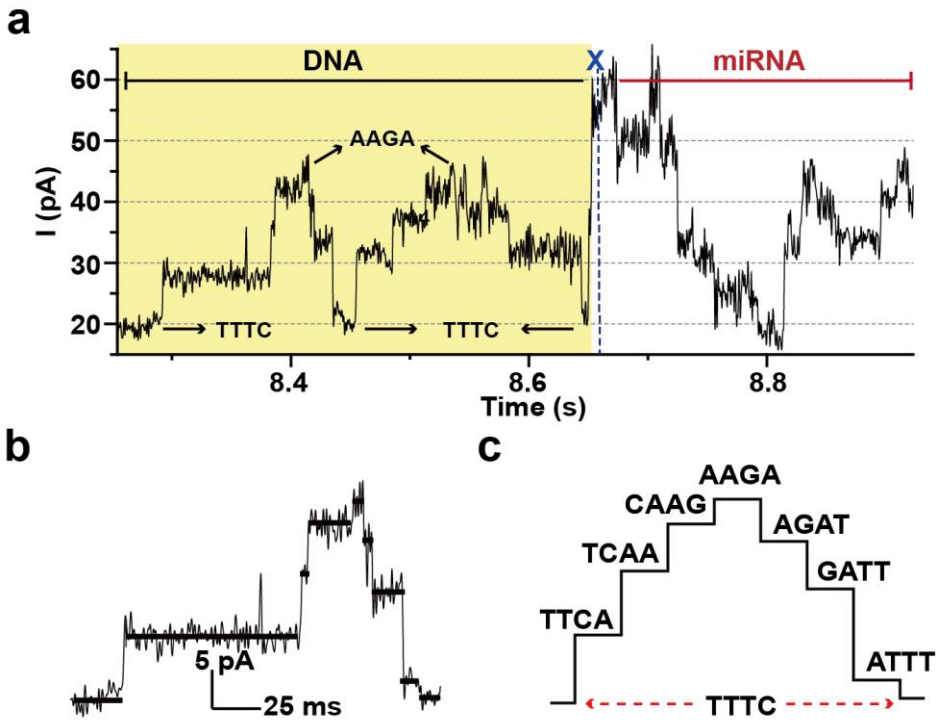

Figure S2: Design of the DNA segment within the chimeric template, Related to Figure 1. **a)** A representative current trace acquired by sequencing DNA-miR-21 using NIPSS. The trace segments that correspond to reading DNA, the abasic spacer and miRNA are marked appropriately. The purpose of including the DNA segment, which is designed on the 5'-end of the chimeric template strand **(Table S1)**, is twofold. First, it acts as a drive strand, which can be enzymatically ratcheted by the phi29 DNAP against the electrophoretic force, guarantees that the miRNA segment can be sequenced by nanopores. Second, by including two sequence repeats of "AGAACTTT" (5'-3') in the DNA segment **(Table S1)**, a unique trace pattern of two triangular wave (region marked with yellow shade) will appear ahead of the miRNA reading, which helps to recognize the initiation of a NIPSS event. Nanopore reading of AAGA and TTTC (3'-5') marked by arrows generates the highest and the lowest residual current among that from all other canonical combinations of DNA quadromers respectively. **b)** The characteristic current signature generated by the DNA segment. The demonstrated trace was extracted from the first repetitive cycle of DNA segment in **a**. Scale bar: 5 pA/25 ms. **c)** The extracted current steps from **b** with aligned quadromer sequences. The sequencing steps correspond to different quadromer readings during NIPSS, in which AAGA and TTTC (3'-5') show the highest and lowest current step, respectively.

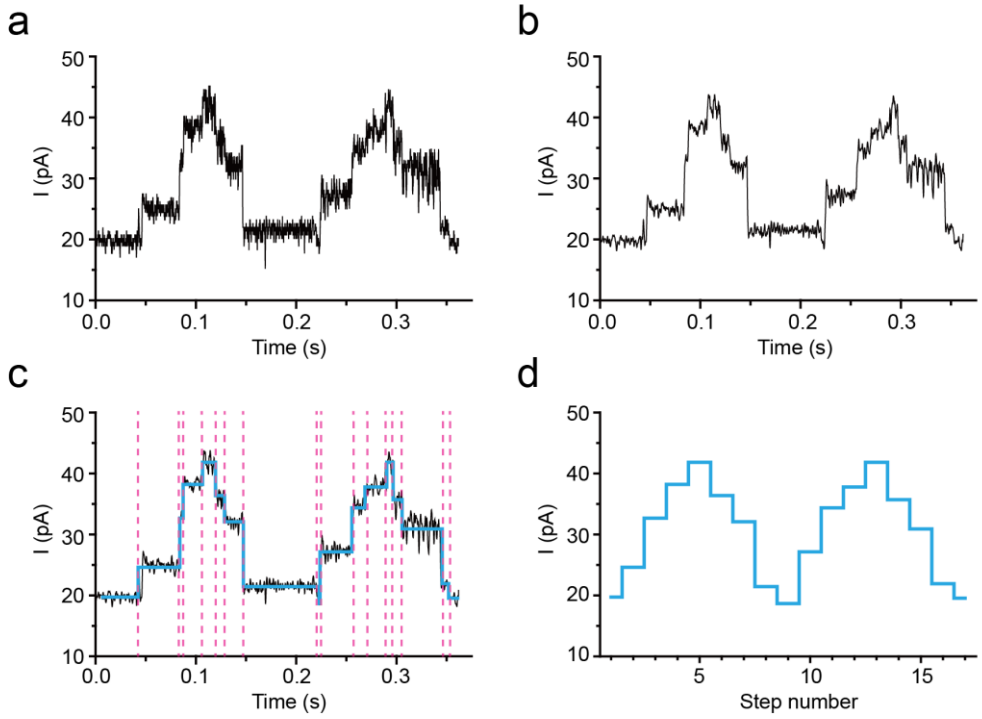

Figure S3: Squiggle plot generation, Related to Figure 1. a) A demonstrative raw nanopore sequencing data. The trace was acquired by a Digidata 1550B digitizer (Molecular Devices) with a 25 kHz sampling rate and low-pass filtered at 5 kHz. **b)** Post-acquisition signal processing. The raw sequencing trace in **a** was further digitally filtered by a low pass Gaussian filtered with a 500 Hz cutoff frequency. Noise at high frequency is significantly reduced after this step. Step transitions resulted from nanopore sequencing is clearly visible in the trace. **c)** Trace segmentation. Step transitions within the trace were automatically detected, as marked with pink dashed lines. Mean values of event steps were separately derived, as marked with blue lines. **d)** Squiggle plot. The squiggle plot was generated by plotting mean values of each event step according to their order of appearance.

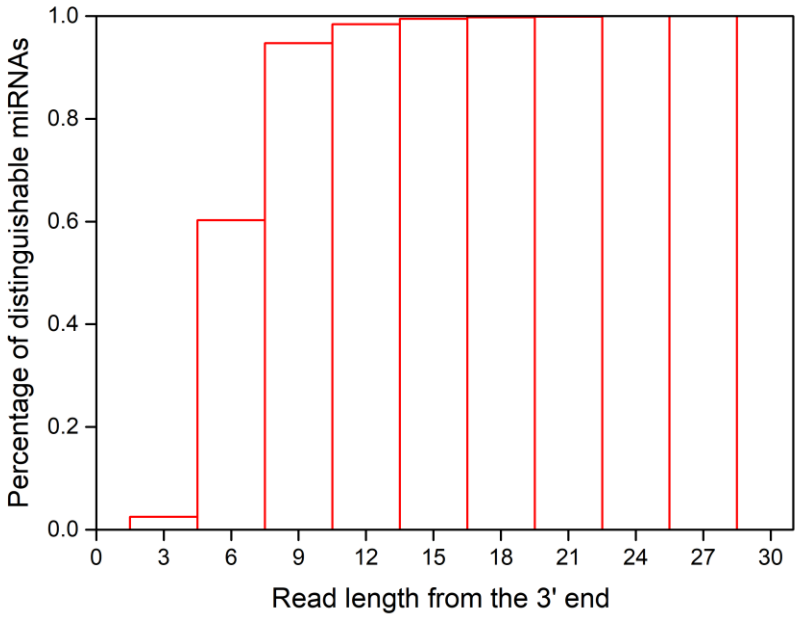

Figure S4: The distinguishable human miRNAs by NIPSS, Related to Figure 1. The sequences of all identified mature human miRNAs were downloaded from miRbase (http://www.mirbase.org/) to form an archive for follow-up analysis. By the time this article is written, this archive contains 2656 human mature miRNAs. It should be noted that some miRNAs share completely identical bases in this archive. For example, hsa-miR-199a-3p and hsa-miR-199b-3p has an identical sequence. These miRNAs originate from either distinct pre-miRNAs or identical pre-miRNAs found in different genome loci (Zhong et al., 2019). By excluding these types of miRNAs with identical sequences, 23 miRNAs have been deleted from the archive, forming an archive of 2633 miRNAs, each with a unique sequence. By reading a different length of nucleotides from their 3' ends, the percentage of distinguishable miRNAs were evaluated. Here, a distinguishable miRNA is counted when this miRNA sequence with a particular read length from their 3' end is different from any other miRNAs in the archive. According to this test, it has been evidenced that by reading the first 15 nucleotides from their 3' end, 99.5% of human miRNA become distinguishable **(Table S2)**.

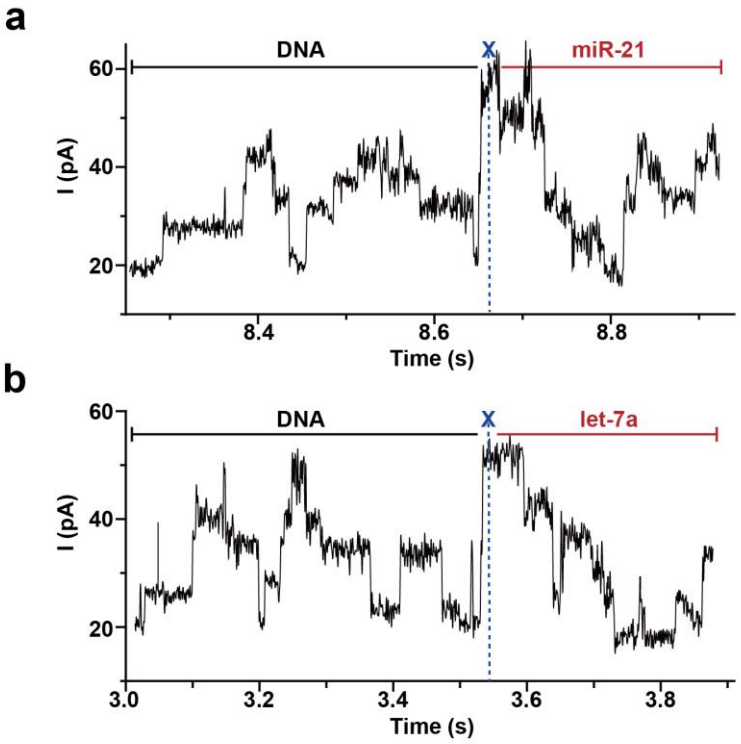

Figure S5: Identification of miR-21 and let-7a by NIPSS, Related to Figure 2. MiRNA identities can be directly recognized by analyzing the miRNA part of the NIPSS signal. **a)** A representative current trace from DNA-miR-21 sequencing. **b)** A representative current trace from DNA-let-7a sequencing. The initiation of miRNA sequencing is indicated by blue dashed lines, where an abasic spacer (X) is read by the nanopore. The signal patterns of the DNA segment show high similarities since the sequence of the DNA drive-strand is identical. Whereas, the miRNA segment of the signal shows remarkable differences between the demonstrated NIPSS events.

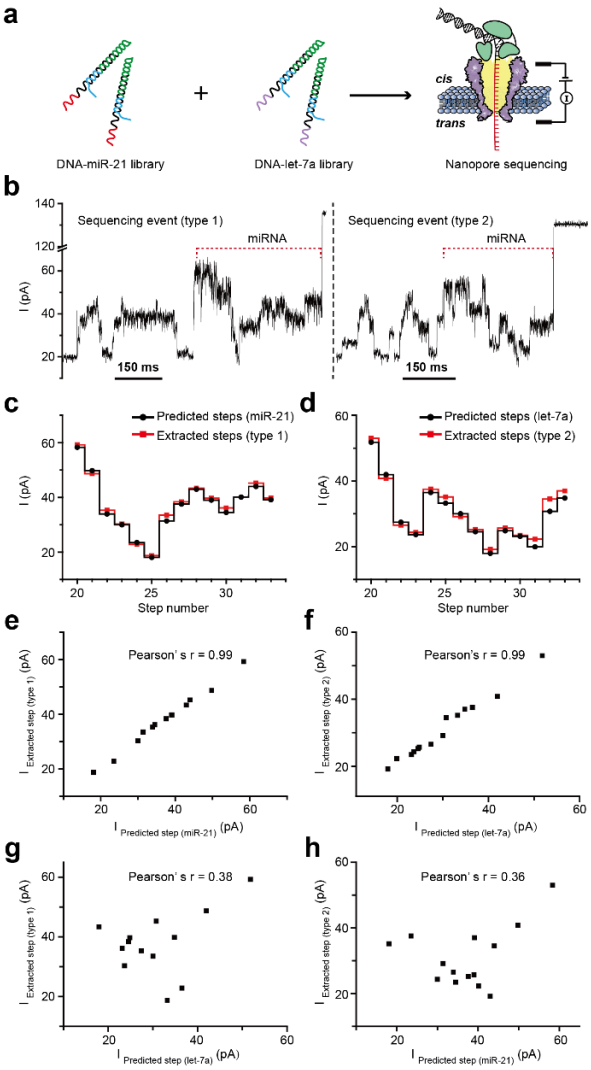

Figure S6: Discrimination of DNA-miR-21 and DNA-let-7a from a mixture, Related to Figure 2. a) The schematic diagram of NIPSS miRNA sequencing from a mixture of analyte. The sequencing library complex was respectively prepared from DNA-miR-21 and DNA-let-7a with a 5 nM final concentration for each composite. **b)** Representative raw sequencing traces acquired from a mixture of DNA-miR-21 and DNA-let-7a measured by the same nanopore**.** Two discriminable types of sequencing events (type 1 and 2), which differs in their miRNA segments (red dashed lines), were clearly recognized. Steps of transition in miRNA segments of each event were extracted as described in **Fig. S3** to form squiggle plots marked as extracted steps in **c** and **d**. The predicted steps of miR-21 and let-7a were respectively created from mean values of sequencing steps acquired from multiple independent miR-21 and let-7a events as demonstrated in **Fig. 2c**. The extracted steps from type 1 or type 2 respectively show strong resembalance with predicted steps from miR-21 or let-7a. To quantitatively evaluate their correlation, results in **c** and **d** were respectively plotted in **e** and **f**, from which the extracted value of one type of event and their predicted values were taken as two sets of variables (x_i, y_i) indexed by i. Pearson correlation coefficient (Pearson's r) was calculated according to the equation $r = \sum_{i=1}^{n}(x_i - \bar{x})\,(y_i - \bar{y}) / \sqrt{\sum_{i=1}^{n}(x_i - \bar{x})^2}\sqrt{\sum_{i=1}^{n}(y_i - \bar{y})^2}$, from which $\bar{x} = (1/n)\sum_{i=1}^{n} x_i$ and of $\bar{y} = (1/n)\sum_{i=1}^{n} y_i$. The Pearson's r between results of type 1 event and

miR-21 or between results of type 2 event and let-7a are both 0.99, indicating a strong linear correlation between. On the other side, as demonstrated in **g** and **h**, extremely weak correlations were observed between type 1 event and let-7a or between type 2 event and miR-21. The reported Pearson's r are for are 0.38 **(g)** and 0.36 **(h)**.

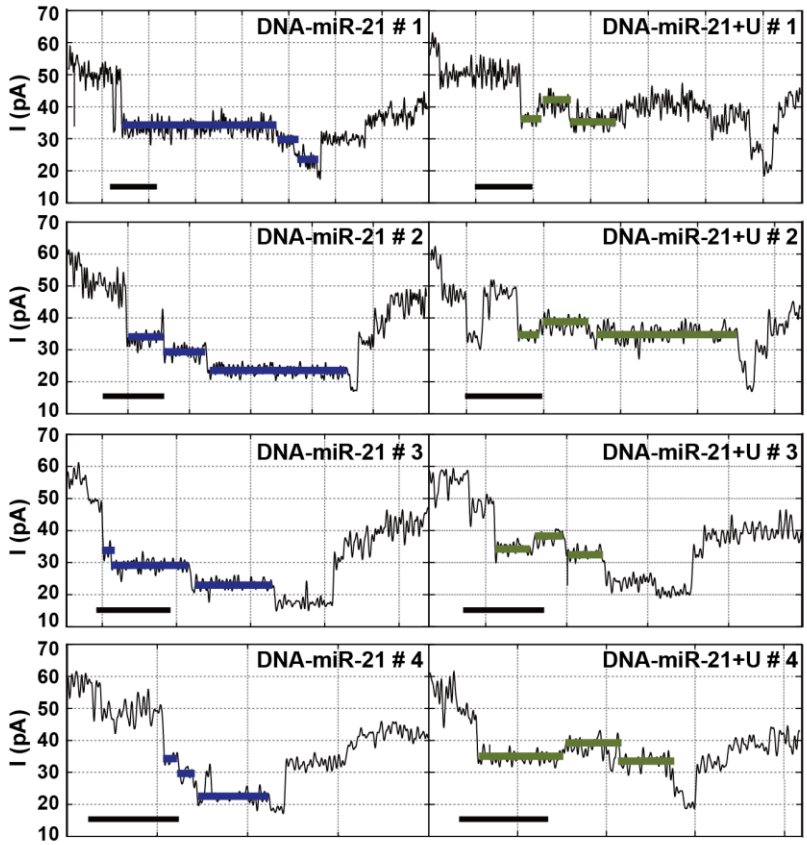

Figure S7: Representative current traces for isomiRs discrimination, Related to Figure 3. Each panel shows individual trace segments, which correspond to the miRNA part of the nanopore sequencing signal of DNA-miR-21 (left) and DNA-miR-21+U (right). Current steps with significant deviations between analytes are indicated by solid lines (blue for miR-21 and yellow for miR-21+U). The duration time for each nanopore sequencing step is stochastic. Scale bar: 50 ms.

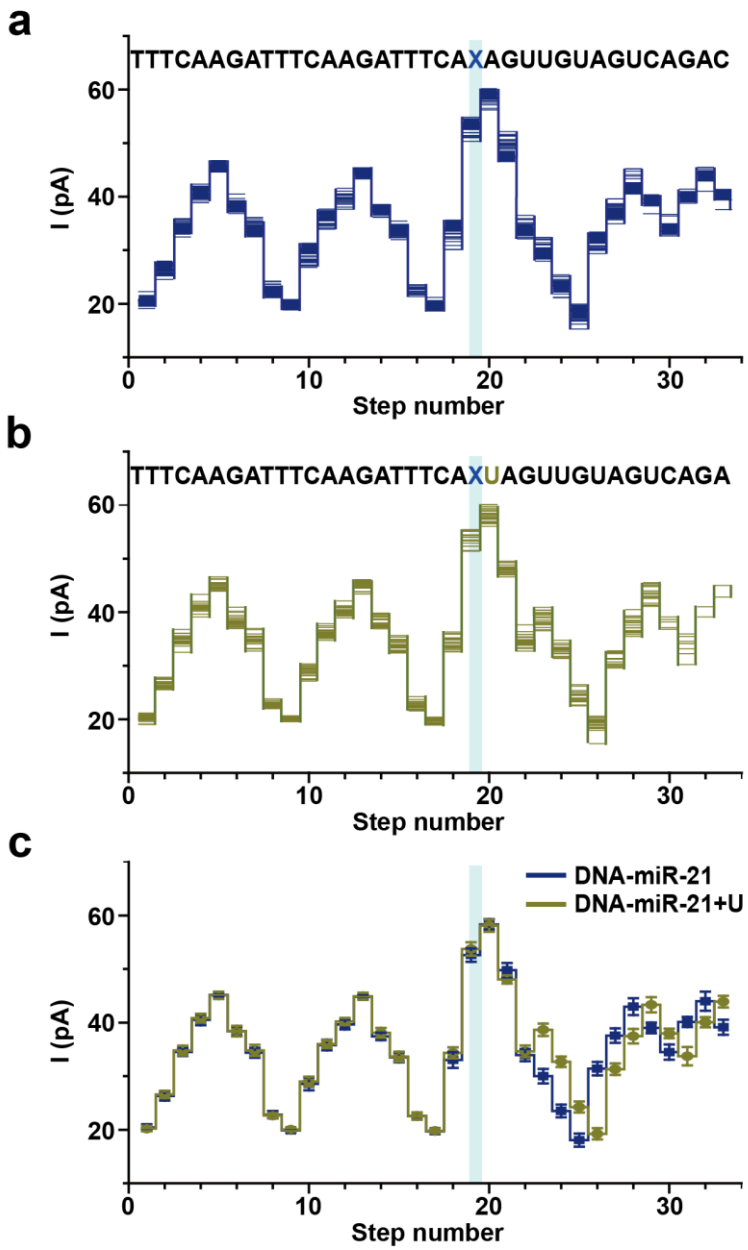

Figure S8: Statistical comparison between DNA-miR-21 and DNA-miR-21+U, Related to Figure 3. a) Overlay of extracted current steps from multiple DNA-miR-21 events (N=24). **b)** Overlay of extracted current steps from multiple DNA-miR-21+U events (N=24). The correlated sequences for each sequence are demonstrated on top of the plots in **(a-b)** where an abasic site (X) is located between DNA and miRNA. **c)** Consensus comparison of sequencing signals between DNA-miR-21 and DNA-miR-21+U. Mean and standard deviations extracted from **a** and **b**. Here, a uridine monophosphate insertion has generated an additional current step when reading DNA-miR-21+U in reference to that of DNA-miR-21. Consequently, the signal pattern from DNA-miR-21+U is shifted by 1 nucleotide. The blue strip in **(a-c)** represents the quadromer reading of TCAX, which is the first quadromer containing the abasic site read by NIPSS.

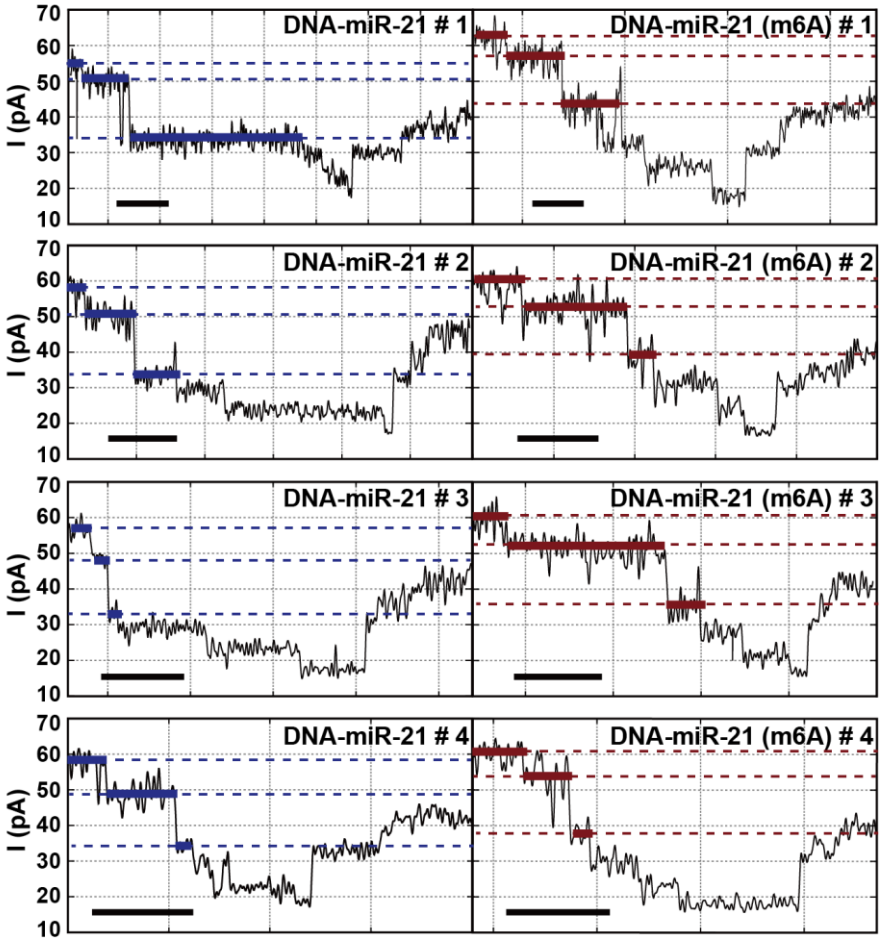

Figure S9: Representative current traces for m6A modification detection, Related to Figure 4. The sequence contexts between DNA-miR-21 and DNA-miR-21(m6A) differ with only one m6A modification **(Table S1)**. Each panel shows individual trace segments, which correspond to the miRNA part of the sequencing signal of DNA-miR-21 (left) and DNA-miR-21(m6A) (right). Current steps with significant deviations between analytes are indicated by solid lines. These level differences could also be recognized from the dashed reference lines. The duration time for each nanopore sequencing step is stochastic. Scale bar: 50 ms.

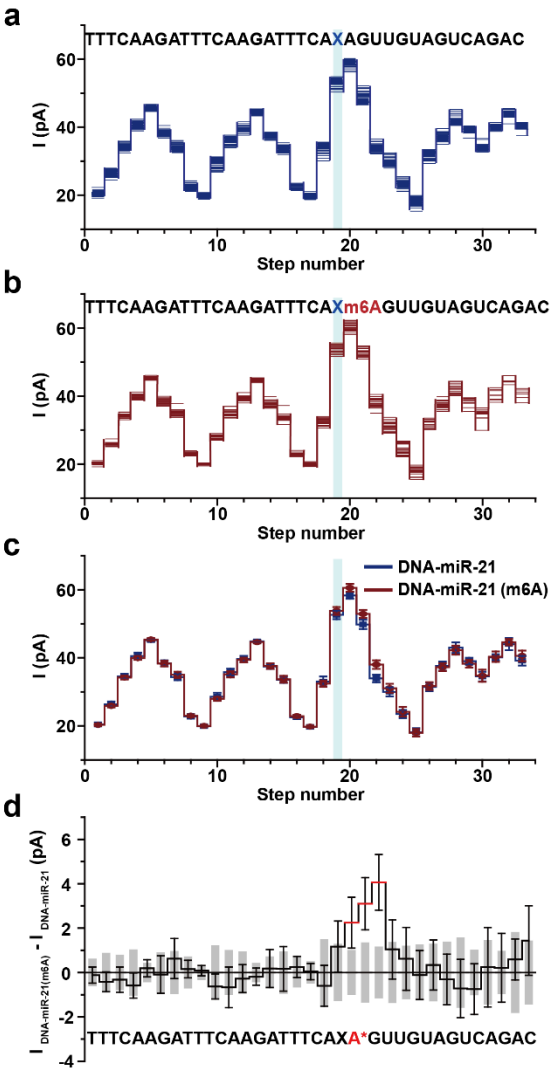

Figure S10: Statistical signal variation between DNA-miR-21 and DNA-miR-21(m6A), Related to Figure 4. a) Overlay of current steps extracted from multiple DNA-miR-21 events (N=24). **b)** Overlay of current steps extracted from multiple DNA-miR-21(m6A) events (N=24). Each current step in **(a-b)** represents the mean current values of each quadromer reading. The correlated sequences are shown above the plots. The "X" within the sequence stands for the abasic site located between the DNA and the miRNA segment of the chimeric template. **c)** Demonstration of different current patterns generated from two DNA-miRNA strands. The average current values and error bars are created from current level traces exhibited in **a** and **b**. The blue strips in **(a-c)** represent the quadromer reading of TCAX, which is the first quadromer containing the abasic site when read by NIPSS. **d)** Statistical current differences between DNA-miR-21 and DNA-miR-21(m6A). Mean current values in **c** were used to construct the current difference map, where the value of $I_{DNA-miR-21(m6A)} - I_{DNA-miR-21}$ is displayed by a black solid line. The standard deviation of signals from DNA-miR-21 is shown with gray columns. The standard deviation of signals from DNA-miR-21(m6A) is demonstrated with black bars. Signal variations caused by m6A modification are shown as three red lines. The sequence of the strand is aligned below the figure, where A* (red) represents either A or m6A in the sequence.

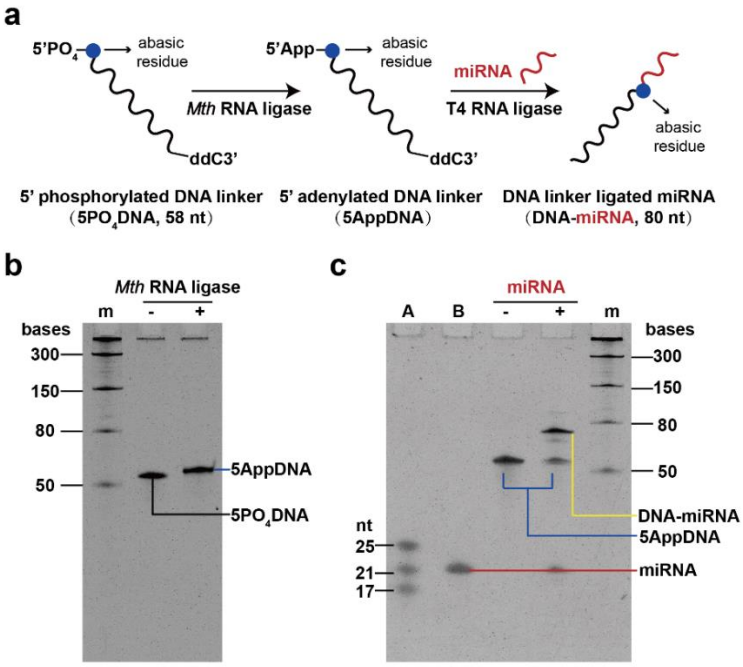

Figure S11: Enzymatic ligation between DNA and RNA, Related to Figure 1. a) A schematic diagram of enzymatic ligation. The reaction starts with a 58 nt DNA linker ($5PO_4$DNA), which has a dideoxycytosine (ddC) on its 3' end and a phosphorylated abasic residue on its 5' end. The abasic site is indicated by blue dot. After treatment with the *M*th RNA ligase (New England Biolabs), the 5' end of the DNA linker is adenylated (5AppDNA). To minimize non-specific ligation, T4 RNA ligase 2 truncated K227Q mutant (T4 Rnl2tr, New England Biolabs) was chosen, which specifically ligates the 5' end of the pre-adenylated DNA linker (5AppDNA) with the 3' end of target miRNA. **b)** Characterization of DNA adenylation by 15% polyacrylamide (PAGE)-urea gel. The adenylation reaction was performed by mixing the following components: 200 pmol $5PO_4$DNA, 4 µL 10x 5' DNA adenylation buffer, 4 µL 1 mM ATP, 4 µL *M*th RNA liagse and nuclease-free H_2O to a final volume of 40 µL. The reaction was incubated at 65 ^oC for 1 h and heat inactivated by incubation at 85 ^oC for 5 min. The reaction product 5AppDNA was purified by ethanol precipitation. Lane + and lane – stands for samples that were incubated with *M*th RNA ligase or not, respectively. Lane m stands for the Low Range ssRNA Ladder (New England Biolabs). 5' adenylation results in slight upshift of the band during gel electrophoresis. **c)** Characterization of DNA-miRNA ligation. Enzymatic ligation results were characterized by 15% PAGE-Urea gel electrophoresis. The ligation reaction was performed by mixing the following components: 5.0 µL 50% (w/v) PEG 8000, 2 µL 10x RNA ligase buffer, 20 pmol 5AppDNA, 10 pmol miRNA, 1 µL T4 Rnl2tr, nuclease-free water to a final volume of 20 µL. The reaction was incubated at 4 °C for 24 h and heat inactivated by incubation at 65 °C for 20 min. Lane A indicates the microRNA Marker (New England Biolabs). Lane B stands for the miR-21 strand. Lane - stands for the 5AppDNA. Lane + stands for the ligation product. Lane m stands for the Low Range ssRNA Ladder (New England Biolabs). An extra, high molecular weight band was detected in lane m, which is the ligated DNA-miRNA chimeric strand.

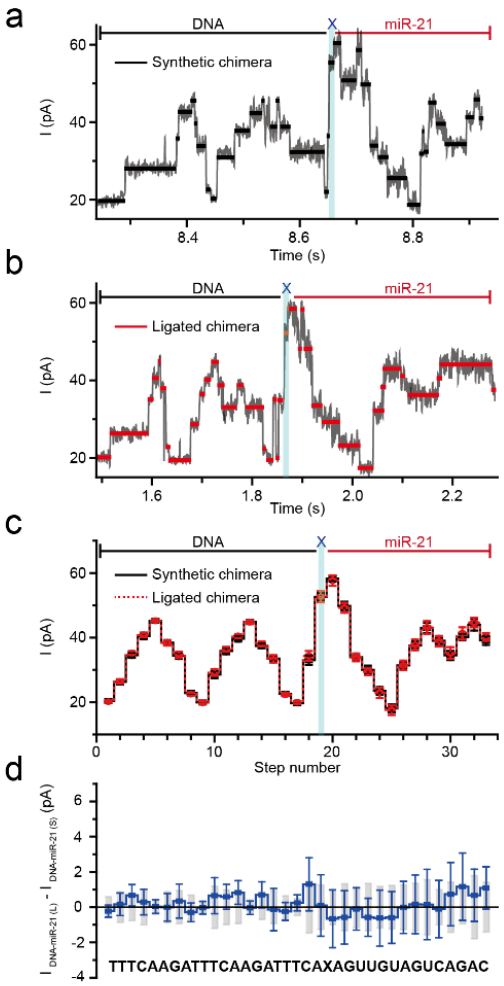

Figure S12: NIPSS sequencing of DNA-miR-21 from the ligated chimera, Related to Figure 1. a) A representative raw trace from NIPSS sequencing of the synthetic DNA-miR-21 chimera. **b)** A representative raw trace from NIPSS sequencing of the ligated DNA-miR-21 chimera. The DNA and miRNA segments of the trace were respectively marked with black and red lines. The trace segment of reading the abasic residue (X) was marked with a blue stripe. Solid lines over the traces in **(a-b)** represent the extracted mean current values of the signal plateau. The demonstrated results were acquired with an aqueous buffer of 0.3 M KCl, 10 mM HEPES/KOH, 10 mM $MgCl_2$, 10 mM $(NH_4)_2SO_4$ and 4 mM DTT at pH 7.5. **c)** An overlay of current steps between two DNA-miR-21 chimeras. Results in the squiggle plots were respectively acquired from either the synthetic or the ligated DNA-miR-21 chimera. The mean and standard deviations values were respectively created from 20 independent sequencing events similar to those shown in **a** and **b**. All steps show a strong resemblance, indicating that the enzymatically ligated chimera was successfully sequenced by the NIPSS configuration. **d)** Statistical current differences between the synthetic DNA-miR-21 chimera and the ligated DNA-miR-21 chimera. Mean current values in **c** were used to construct the current difference map, where the value of $I_{DNA-miR-21(L)} - I_{DNA-miR-21(S)}$ is displayed by a blue solid line. Here, the "L" or "S" label respectively represents the ligated chimera or the synthetic chimera. The standard deviation values from the synthetic DNA-miR-21 chimera were shown with gray columns. The standard deviation values from the ligated DNA-miR-21 chimera were

demonstrated with blue bars. The mean current differences appear negligible between the two sources of DNA-miR-21 chimeras, indicating that the enzymatic ligation described in **Fig. S11** could be used to construct NIPSS sequencing libraries from natural miRNAs.

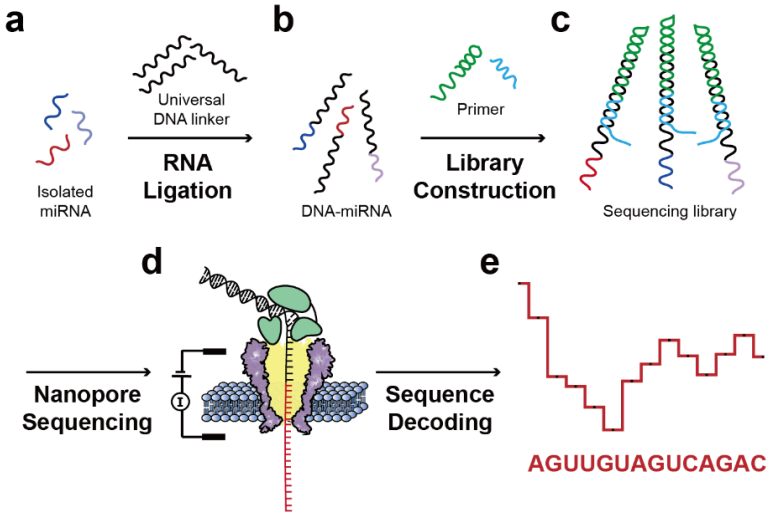

Figure S13: A proposed strategy to directly sequence miRNA from natural resources, Related to Figure 1. a-c) Schematic diagram of NIPSS sequencing library preparation with isolated miRNA from natural resources. Isolated miRNAs **a)** could be ligated to form DNA-miRNA chimeric strands **b)** and subsequently form sequencing libraries **c)** by thermal annealing. **d)** Direct miRNA sequencing is carried out as described in this paper. **e)** Current step transitions during NIPSS reading of miRNA could be decoded into RNA sequences for downstream clinical diagnosis or bioinformatics investigations.

Table S1: Nucleic acid sequences used in this study, Related to Figure 1, 2, 3 and 4, and to Figure S11 and S12.

Construct	Sequence (5'-3')
DNA-miR-21	UAGCUUAUCAGACUGAUGUUGAXACTTTAGAACTTTAGAACTTTTCAGATCTC ACTATCGCATTCTCATGCAGGTCGTAGC
DNA-let-7a	UGAGGUAGUAGGUUGUAUAGUUXACTTTAGAACTTTAGAACTTTTCAGATCTC ACTATCGCATTCTCATGCAGGTCGTAGC
DNA-miR-21+U	UAGCUUAUCAGACUGAUGUUGAUXACTTTAGAACTTTAGAACTTTTCAGATCT CACTATCGCATTCTCATGCAGGTCGTAGC
DNA-miR-21 (m6A)	UAGCUUAUCAGACUGAUGUUGm6AXACTTTAGAACTTTAGAACTTTTCAGATC TCACTATCGCATTCTCATGCAGGTCGTAGC
Primer	GCGTACGCCTACGGTTTTCCGTAGGCGTACGCGCTACGACCTGCATGAGAATG C
Blocker	GATAGTGAGATCTGATTTCCCAAATTTAAA-cholesterol
DNA linker	PO_4- XACTTTAGAACTTTAGAACTTTTCAGATCTCACTATCGCATTCTCATGCAGGT CGTAG-dideoxyC
miR-21	UAGCUUAUCAGACUGAUGUUGA

Notes:

1. All miRNA segments of the sequence contexts are underlined.
2. Primer/Template duplex regions in the chimeric template strand are indicated by blue letters.
3. Blocker/Template duplex regions in the chimeric template strand are indicated by red letters.
4. The "X" letter represents the abasic site.
5. PO_4 stands for the 5' phosphate group.
6. DideoxyC stands for a 3' dideoxycytosine.

Table S2: The values of distinguishable ratio for various read length from 3' end of miRNAs, Related to section "Direct miRNA sequencing using NIPSS" in main-text, and to Figure 1.

RNA read length from the 3' end	Counts of undistinguishable miRNAs	Counts of distinguishable miRNAs	Distinguishable ratio (%)
3	2567	66	2.51
6	1045	1588	60.31
9	138	2495	94.76
12	41	2592	98.44
15	14	2619	99.47
18	6	2627	99.77
21	2	2631	99.92
24	0	2633	100
27	0	2633	100

Table S3: Current values of all 4-nucleotides sequence contexts for isomiRs, Related to Figure 3.

Level number	miR-21			miR-21+U		
	Sequence quadromers (3'-5')	Mean I value (pA)	Standard Deviation (pA)	Sequence quadromers (3'-5')	Mean I value (pA)	Standard Deviation (pA)
1	TTTC	20.4	0.6	TTTC	20.2	0.5
2	TTCA	26.3	0.9	TTCA	26.6	0.7
3	TCAA	34.5	0.8	TCAA	34.8	0.9
4	CAAG	40.5	1.0	CAAG	40.9	0.8
5	AAGA	45.2	0.4	AAGA	45.1	0.7
6	AGAT	38.4	0.9	AGAT	38.4	1.0
7	GATT	34.4	0.9	GATT	34.8	1.0
8	ATTT	22.8	0.7	ATTT	22.6	0.5
9	TTTC	19.9	0.3	TTTC	20.0	0.3
10	TTCA	28.6	1.2	TTCA	29.0	0.9
11	TCAA	35.8	1.0	TCAA	36.0	0.7
12	CAAG	39.7	0.9	CAAG	40.2	0.7
13	AAGA	44.8	0.4	AAGA	44.9	0.7
14	AGAT	37.4	0.7	AGAT	38.1	0.9
15	GATT	33.5	0.9	GATT	33.7	0.9
16	ATTT	22.6	0.6	ATTT	22.5	0.7
17	TTTC	19.7	0.5	TTTC	19.8	0.4
18	TTCA	33.0	1.5	TTCA	34.4	1.0
19	TCAX	52.6	1.3	TCAX	53.7	1.3
20	CAXA	58.3	1.0	CAXU	58.1	1.1
21	AXAG	49.8	1.3	AXUA	48.0	0.8
22	XAGU	33.9	1.1	XUAG	34.7	1.1
23	AGUU	30.0	1.3	UAGU	38.7	1.2
24	GUUG	23.5	1.2	AGUU	32.7	1.0
25	UUGU	18.1	1.2	GUUG	24.2	1.0
26	UGUA	31.4	1.3	UUGU	19.2	1.0
27	GUAG	37.6	1.4	UGUA	31.3	1.1
28	UAGU	43.0	1.6	GUAG	37.5	1.4
29	AGUC	39.0	1.0	UAGU	43.3	1.4
30	GUCA	34.5	1.4	AGUC	38.0	0.9
31	UCAG	40.1	0.9	GUCA	33.7	1.7
32	CAGA	44.0	1.8	UCAG	40.1	1.0
33	AGAC	39.1	1.4	CAGA	43.9	1.1

Transparent Methods

Materials

Potassium chloride (KCl), sodium chloride (NaCl), sodium hydrogen phosphate (Na_2HPO_4) and sodium dihydrogen phosphate (NaH_2PO_4) were obtained from Aladdin (China). Magnesium chloride ($MgCl_2$) was from Macklin. Ammonium sulfate $(NH_4)_2SO_4$ was from Xilong Scientific. 4-(2-hydroxyethyl)-1-piperazine ethanesulfonic acid (HEPES) was from Shanghai Yuanye Bio-Technology (China). Ammonium persulfate, kanamycin sulfate, dl-dithiothreitol (DTT), dioxane-free isopropyl-β-D-thiogalactopyranoside (IPTG), N,N,N',N'-Tetramethyl- ethylenediamine (TEMED) and imidazole were from Solarbio (China). Ethylene- diaminetetraacetic acid (EDTA), pentane, hexadecane and Genapol X-80 were from SIGMA-ALDRICH. 1,2-diphytanoyl-sn-glycero-3-phosphocholine (DPhPC) was from Avanti Polar Lipids. Urea was from BIOSHARP. Acrylamide was from Sangon Biotech. The Low Range ssRNA Ladder (#N0364S), microRNA Marker (#N2102S), RNA loading dye (#B0363S), Nuclease-free Water (#B1500S), T4 RNA ligase 2 truncated K227Q mutant (T4 Rnl2tr; #M0242S), phi29 DNA Polymerase (#M0269S), deoxynucleotide (dNTP) solution mix (#N0447S) and the 5' DNA Adenylation kit (E2610S) were from New England Biolabs. *E. coli* strain BL21 (DE3) was from Biomed (China). Luria-Bertani (LB) agar and LB broth were from Hopebio (China).

All HPLC-purified DNA oligonucleotides, including DNA-miRNA template strands, primer, blocker, DNA linker and miR-21 **(Table S1)** were custom synthesized by Genscript (New Jersey, USA).

Methods

1. The construction of miRNA sequencing library.

The sequencing library for NIPSS is thermally annealed from three separate nucleic acid strands: the chimeric template, the primer and the blocker **(Fig. 1a, Table S1)**. These three strands were mixed with a 1:1:2 molar ratio in an aqueous buffer (0.3 M KCl, 10 mM HEPES/KOH, 10 mM $MgCl_2$, 10 mM $(NH_4)_2SO_4$). Thermal annealing was carried out by incubating the mixture at 95 °C for 2 min and program cooled down to 25 °C with a rate of -5 °C/min. For optimum sequencing data production, the thermal annealed sequencing library should be immediately used in subsequent NIPSS measurements.

2. The preparation of a biological nanopore.

The MspA mutant (D90N/D91N/D93N/D118R/D134R/E139K) nanopore (Butler et al., 2008) was expressed with *E. coli* BL21 (DE3) and purified with nickel affinity chromatography as described previously (Wang et al., 2018; Yan et al., 2019). This MspA mutant, which is the sole MspA nanopore discussed in this paper, is named MspA, if not otherwise stated. Briefly, the constructed plasmid gene for MspA was heat-shock transformed into *E. Coli* BL21 (DE3). Afterwards, the cells were grown in LB medium to an OD_{600}=0.7, induced with 1 mM IPTG and

shaken (180 rpm) overnight at 16 °C. The cells were harvested by centrifugation (4000 rpm, 20 min, 4 °C). The collected pellet was re-suspended in the lysis buffer (100 mM Na_2HPO_4/NaH_2PO_4, 0.1 mM EDTA, 150 mM NaCl, 0.5% (w/v) Genapol X-80, pH 6.5) and heated to 60 °C for 10 min. The suspension was cooled on ice for 10 min and centrifuged at 4 °C for 40 min at 13,000 rpm. After syringe filtration, the supernatant was loaded to a nickel affinity column (HisTrapTM HP, GE Healthcare). The column was first eluted with buffer A (0.5 M NaCl, 20 mM HEPES, 5 mM imidazole, 0.5% (w/v) Genapol X-80, pH=8.0) and further eluted with a linear gradient of imidazole (5 mM-500 mM) by mixing buffer A with buffer B (0.5 M NaCl, 20 mM HEPES, 500 mM imidazole, 0.5% (w/v) Genapol X-80, pH=8.0). The eluted fractions were further characterized by SDS-polyacrylamide gel electrophoresis (PAGE) and the desired protein was identified. The identified fraction was immediately used for NIPSS experiments or stored at -80 °C for long term storage.

3. NIPSS experiments.

NIPSS experiments were carried out as described previously (Yan et al., 2019). Briefly, the electrolyte buffer (0.3 M KCl,10 mM HEPES/KOH, 10 mM $MgCl_2$, 10 mM $(NH_4)_2SO_4$ and 4 mM DTT at pH 7.5) were separated by a 1,2-diphytanoyl-sn-glycero-3-phosphocholine (DPhPC) lipid membrane (Avanti Polar Lipids) into *cis* and *trans* compartments. Both compartments were in contact with separate Ag/AgCl electrodes and connected to an Axopatch 200B patch clamp amplifier (Molecular Devices) to form a circuit, while the *cis* compartment is electrically grounded. Purified MspA nanopores were added in *cis* and spontaneously inserted into the membrane. With a single pore inserted **(Fig. 1b)**, the sequencing library, dNTPs and phi29 DNAP could be added into *cis* and stirred magnetically to reach final concentrations of 5 nM, 250 μM and 1 nM, respectively. Nanopore sequencing was initiated by holding an applied voltage at +180 mV. All electrophysiology recordings were acquired with a Digidata 1550B digitizer (Molecular Devices) with a 25 kHz sampling rate and low-pass filtered at 5 kHz. All NIPSS experiments were performed at room temperature (22 ±1 °C).

4. Data analysis.

Nanopore sequencing events were extracted from raw electrophysiology traces according to their unique pattern of signal transitions. The extracted events were low pass filtered at 500 Hz using Clampfit 10.7 (Molecular Devices) for further analysis **(Fig. S3)**. The sequencing steps, which represents signal plateau transitions within traces were fragmented. The average current for each step was calculated and finally extracted from sequencing events.

Supplemental References

Butler, T.Z., Pavlenok, M., Derrington, I.M., Niederweis, M., and Gundlach, J.H. (2008). Single-molecule DNA detection with an engineered MspA protein nanopore. Proc. Natl. Acad. Sci. USA *105*, 20647-20652.

Wang, Y., Yan, S., Zhang, P., Zeng, Z., Zhao, D., Wang, J., Chen, H., and Huang, S. (2018). Osmosis-Driven Motion-Type Modulation of Biological Nanopores for Parallel Optical Nucleic Acid Sensing. ACS Appl. Mater. Interfaces *10*, 7788-7797.

Zhong, X., Heinicke, F., and Rayner, S. (2019). miRBaseMiner, a tool for investigating miRBase content. RNA biology *16*, 1534-1546.